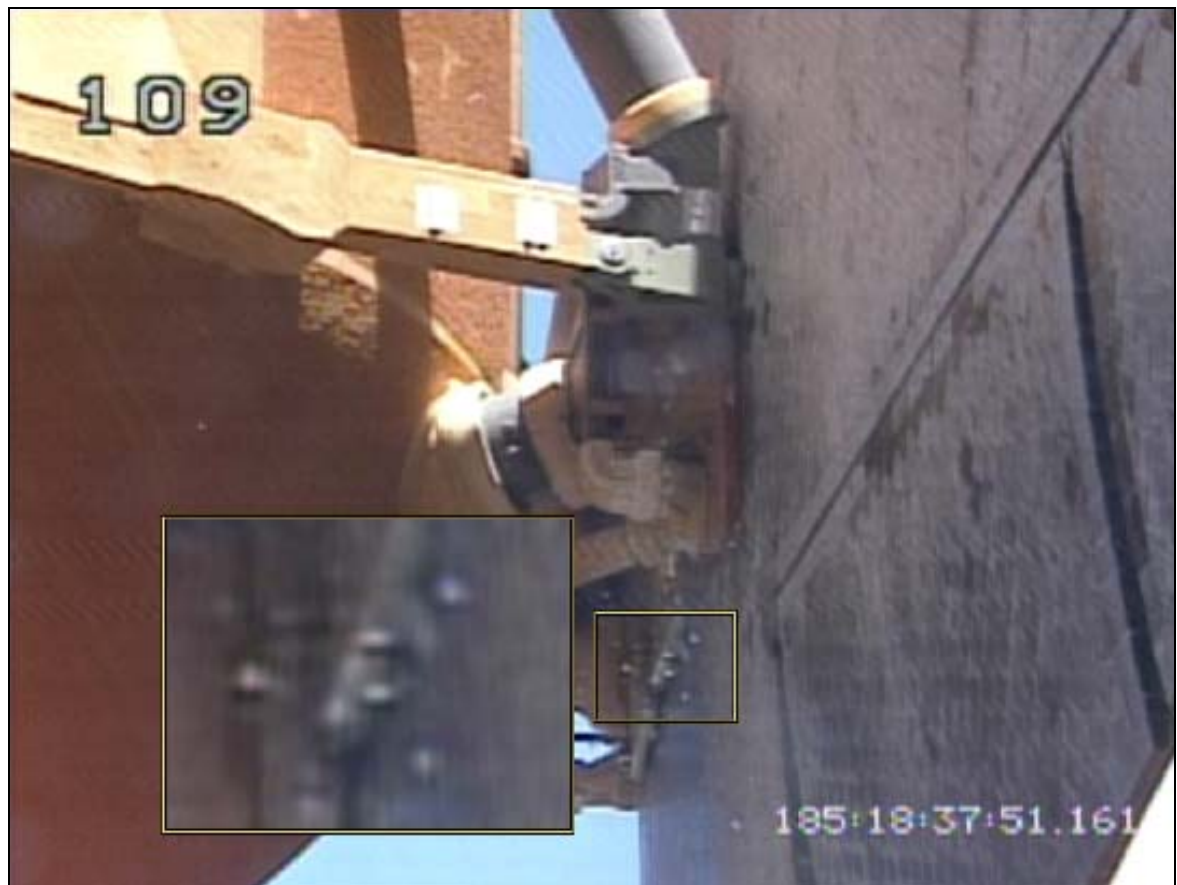




Double Lap Shear Testing of Coating-Modified Ice Adhesion to Space Shuttle Component Surfaces

Michael G. Ferrick, Nathan D. Mulherin, Barry A. Coutermash,
Glenn D. Durell, Leslie A. Curtis, Terry L. St. Clair, Erik S. Weiser,
Roberto J. Cano, Trent M. Smith, Charles G. Stevenson, and
Eloy C. Martinez

December 2006



Cover Photograph: Umbilical ice fall during STS 121 launch, July 2006.
(Photo by JSC Image Science and Analysis Group.)

Double Lap Shear Testing of Coating-Modified Ice Adhesion to Space Shuttle Component Surfaces

Michael G. Ferrick, Nathan D. Mulherin, Barry A. Coutermash, and Glenn D. Durell

*Cold Regions Research and Engineering Laboratory
U.S. Army Engineer Research and Development Center
72 Lyme Road
Hanover, NH 03755-1290*

Leslie A. Curtis

*NASA Engineering and Safety Center
Marshall Space Flight Center, AL*

Terry L. St. Clair

*National Institute of Aerospace
Hampton, VA*

Erik S. Weiser and Roberto J. Cano

*NASA Langley Research Center
Hampton, VA*

Trent M. Smith and Charles G. Stevenson

*NASA John F. Kennedy Space Center
Kennedy Space Center, FL*

Eloy C. Martinez

*Lockheed Martin Space Systems
Marshall Space Flight Center, AL*

Approved for public release; distribution is unlimited

Prepared for National Aeronautics and Space Administration

Abstract: The goals of this experimental program were to optimize the effectiveness of an icephobic coating for use on several Space Shuttle surfaces, to evaluate the effects of adding an ultraviolet light absorber (UVA) on coating performance, and to assess the consistency and durability of the basic coating and its modifications. The double lap shear test was used to quantify ice adhesion performance at a constant temperature of -112°C (-170°F). The experiments used ice that was grown as strong and consistently as possible before being subjected to the extreme temperature decrease. Standardized coating application with a foam brush provided consistent and reproducible surface coverage. The program included 20 tests subdivided in two phases. Phase 1 focused on determining an optimal coating of Rain-X and varying weight fractions of PTFE powders MP-55 and UF-8TA. Ice adhesion to the UF-8TA coatings was similar to that of the uncoated controls. Conversely, the MP-55 coatings produced large reductions in ice adhesion. Through three cycles of phase 1 testing the M4 coating, a mixture of 60% Rain-X with 40% MP-55, was the best and most consistent by a wide margin. As a result, M4 was the basis of all phase 2 mixes. Phase 2 tests sought to verify the effectiveness and durability of the optimal coating for several surfaces on the shuttle and to quantify any changes in effectiveness resulting from the addition of UVA to the coating. The ice adhesion to coated coupons with Koropon, Kapton tape, Kapton film, and Fire-X (fire-retardant paint) surfaces was a small fraction of the adhesion to corresponding uncoated coupons. Rain-X solvent loss during prolonged coating preparation caused a greater increase in ice adhesion than that of adding the UVA. A rapid mixing procedure was developed to minimize this problem. The M4 coating showed outstanding performance and durability through five cycles of ice growth and adhesive failure.

DISCLAIMER: The contents of this report are not to be used for advertising, publication, or promotional purposes. Citation of trade names does not constitute an official endorsement or approval of the use of such commercial products. All product names and trademarks cited are the property of their respective owners. The findings of this report are not to be construed as an official Department of the Army position unless so designated by other authorized documents.

DESTROY THIS REPORT WHEN NO LONGER NEEDED. DO NOT RETURN IT TO THE ORIGINATOR.

Contents

Preface	vi
1 Introduction.....	1
2 Coating Preparation and Application.....	5
3 Sample Preparation, Test, and Program Overview.....	8
4 Data Analysis Methods and Measures	11
5 Phase 1 Program.....	12
6 Phase 1 Results.....	15
Cycle 1	15
Cycles 2 and 3	19
7 Phase 1 Conclusions.....	25
8 Phase 2 Program.....	26
9 Phase 2 Results.....	28
Multiple Surfaces: Uncoated and Cycle 1 Coated	28
Multiple Surfaces and Higher Cycle Coated	32
10 Phase 2 Conclusions.....	41
11 Ice Structure and Fracturing during Cryogenic DLS Testing.....	42
12 Contact Angle and XPS Analyses	47
13 Conclusions.....	50
References.....	53
Report Documentation Page.....	54

Figures and Tables

Figures

Figure 1. STS-114 umbilical area, 13 July 2005 launch attempt	2
Figure 2. STS-114 LO ₂ umbilical area, 13 July 2005 launch attempt	2
Figure 3. STS-115 LO ₂ umbilical area, 23 August 2006 preflight inspection	3
Figure 4. STS-115 LO ₂ umbilical area access from the platform on the launch pad, 23 August 2006 preflight inspection	3
Figure 5. Applicators being evaluated, together with their corresponding coated coupons, and close-up of the foam brush with wooden handle and its corresponding coated coupon	6
Figure 6. Foam brush filled with SILC prior to application of the coating to the coupon surface	7
Figure 7. M4, M5, and control samples in the coldroom at -15°C prior to transport to the test chamber, 30 May 2006	8
Figure 8. Temperatures under the insulated cover, in the surrounding cold box, and in the larger coldroom during growth of three sample sets, 5-7 June 2006	9
Figure 9. M5, U5, and MU coated coupons prior to phase 1 testing	13
Figure 10. Phase 1 (cycle 1) results for all coupon groups: average peak load, average work by strain rate, and average power by strain rate	17
Figure 11. Phase 1 load-time traces of representative tests for the U57 coating, U5 coating, and uncoated controls	18
Figure 12. Average peak load, average work at low strain rate, and average work at high strain rate for all MP-55 coating variations over three cycles of phase 1 testing	20
Figure 13. Average power at low strain rate and at high strain rate for all MP-55 coating variations over three cycles of phase 1 testing	21
Figure 14. Peak load of individual coupons through three cycles of phase 1 testing: M5 and M4	22
Figure 15. Total work of individual coupons through three cycles of phase 1 testing: M5 and M4	22
Figure 16. Comparison of representative load-time traces of cycles 1 and 3: M5 and M4	23
Figure 17. M4 coupons after one, two, and three test cycles	24
Figure 18. Failed Kapton tape and adhesive resulting from uncoated DLS testing	28
Figure 19. Comparison of average measures for uncoated and cycle 1 coated Koropon, Kapton tape, Kapton film, and Fire-X surfaces: peak load, work at low strain rate, and work at high strain rate	30
Figure 20. Load-displacement traces for representative uncoated control tests and Kapton film tests	31
Figure 21. Load-time traces of representative M42, MT, and MT4 tests in cycle 1	32
Figure 22. Load-time traces of representative M42, MT, and MT4 tests in cycle 2	34

Figure 23. Average measures through two cycles for SILC applied to Koropon, Kapton tape, Kapton film, and Fire-X surfaces: peak load, work at low strain rate, and work at high strain rate	35
Figure 24. Coated Kapton film and Kapton tape after two test cycles, Fire-X and MT4 after two test cycles, and MT and M42 after four test cycles	36
Figure 25. Average measures through two or four test cycles comparing M4, M42, MT, and MT4 coatings: peak load, work at low strain rate, and work at high strain rate	38
Figure 26. Peak load and total work of individual M4 coupons through five test cycles	39
Figure 27. Comparison of representative M4 load-time traces for cycles 3 and 5	39
Figure 28. Ice samples from two sides of mold NC with general backlighting and cross-polarized light	43
Figure 29. Ice samples from two sides of mold M4-2(5) with point backlighting and cross-polarized light	44
Figure 30. Ice samples from two K molds with point backlighting and cross-polarized light	45
Figure 31. Near-minimum and near-maximum contact angles for coupons M4-02 after five test cycles, M42-01 after four test cycles, and MT-05 after four test cycles	47

Tables

Table 1. Phase 1 coating compositions	13
Table 2. Double lap shear test program: Phase 1	14
Table 3. Summary of results, Phase 1, Cycle 1	16
Table 4. Summary of results, Phase 1, Cycles 2 and 3	19
Table 5. Double lap shear test program: Phase 2	27
Table 6. Summary of results, Phase 2, Cycle 1	29
Table 7. Summary of results, Phase 2, Cycle 2	33
Table 8. Summary of results, Phase 2, Cycles 3, 4, and 5	37
Table 9. Contact angle summary	48
Table 10. XPS data summary	49

Preface

This report was prepared by Michael G. Ferrick, Environmental Sciences Branch, Cold Regions Research and Engineering Laboratory (CRREL), U.S. Army Engineer Research and Development Center (ERDC), Hanover, NH; Nathan D. Mulherin, Snow and Ice Branch, CRREL/ERDC; Barry A. Coutermash, Applied and Military Engineering Branch, CRREL/ERDC; Glenn D. Durell, Engineering Resources Branch, CRREL/ERDC, Leslie A. Curtis, NASA Engineering and Safety Center, MSFC, AL; Terry L. St. Clair, National Institute of Aerospace, Hampton, VA; Erik S. Weiser and Roberto J. Cano, NASA Langley Research Center, Hampton, VA; Trent M. Smith and Charles G. Stevenson, NASA John F. Kennedy Space Center, FL, and Eloy C. Martinez, Lockheed Martin Space Systems, MSFC, AL.

The authors thank the many members of the NASA ice mitigation team who contributed to the success of this work. Nancy Perron of CRREL prepared thin sections for the ice for the ice structure-fracture analysis, and David Cate of the ERDC Information Technology Laboratory edited the report. Funding to support the CRREL staff on this project was provided under NASA order number NNL05AA401 and is gratefully acknowledged.

The report was prepared under the general supervision of Dr. Terry Sobecki, Chief, Environmental Sciences Branch; Dr. Lance Hansen, Deputy Director; and Dr. Robert Davis, Director, CRREL.

The Commander and Executive Director of ERDC is COL Richard B. Jenkins. The Director is Dr. James R. Houston.

1 Introduction

Ice is one form of debris from the external fuel tank of the space shuttle that can be liberated during launch and cause damage to the shuttle elements. Work to find a coating that would reduce ice formation or adhesion on the external tank (ET) was initially focused on the Koropon-primed aluminum surfaces of the liquid oxygen (LO₂) feed line brackets (DeWeese et al. 2006, Ferrick et al. 2006). The initial challenge was to find a coating material that would reduce ice formation and/or ice adhesion at cryogenic temperatures to the substrate materials characteristic of the bracket surface. The resulting ice release at low speed under gravity and induced vibration loading, very early in the launch, would minimize the damage potential. If the coating were hydrophobic, then the contribution to ice growth by water rundown on the external tank would also be reduced.

Constraints imposed on the coating included durability and tolerance of exposure to wind, rain, sunlight, and multiple cryogenic cycles. In addition, the coating must be compatible with already built hardware and require no disassembly, and the application method must be controlled such that the coating is only applied where needed and not to other areas. The test series conducted by Ferrick et al. (2006) identified the outstanding performer of all candidate coatings, named Shuttle Ice Liberation Coating (SILC), which greatly reduced the ice adhesion strength and satisfied the constraints for bracket application. This coating, a mixture of Rain-X and powdered Teflon, can potentially be applied to other areas on the shuttle system that form ice prior to launch. Such areas include the ET/Orbiter umbilical area shown in Figure 1, the ice frost ramps, and the feed line bellows. Figure 2 provides a close-up of the LO₂ umbilical area showing frost and ice development on insulating foam and Kapton film (orange translucent material) surfaces. Kapton film is cut to fit and taped in place while the shuttle is in the vehicle assembly building (VAB). A closer view of this area is presented in Figure 3, where Fire-X (fire retardant) painted foam can be seen in addition to Kapton film and tape. Icephobic coating application could be done in the VAB or from the platform at the launch pad, where easy access and good lighting exist (Fig. 4).

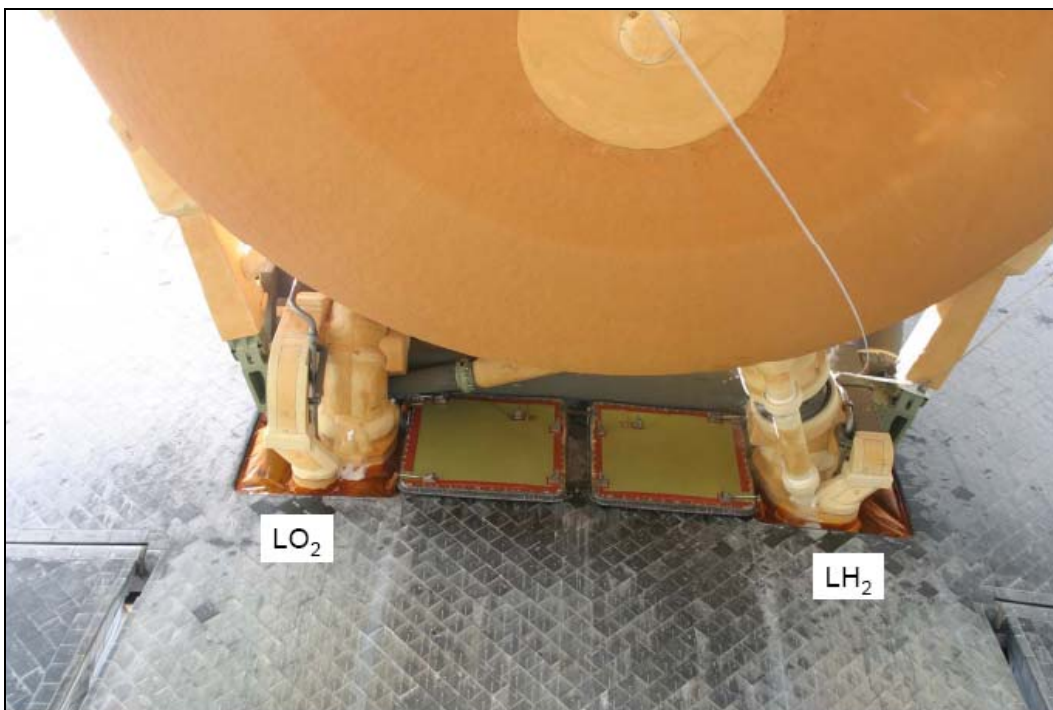


Figure 1. STS-114 umbilical area, 13 July 2005 launch attempt.

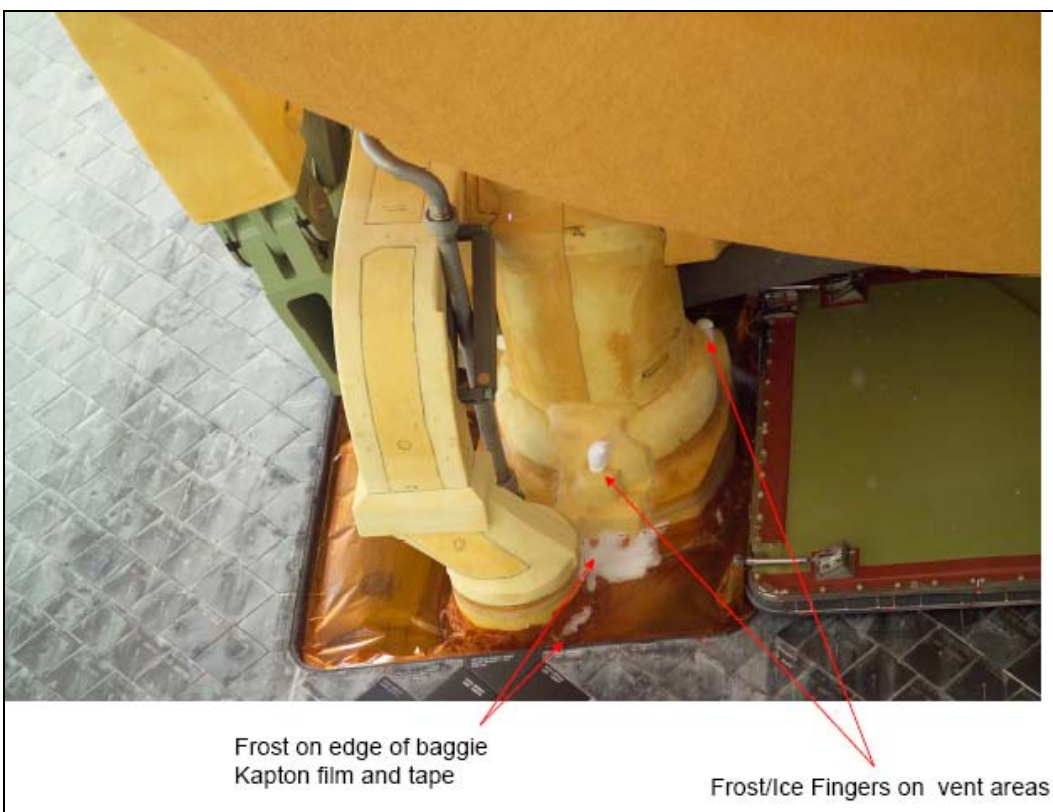


Figure 2. STS-114 LO_2 umbilical area, 13 July 2005 launch attempt.

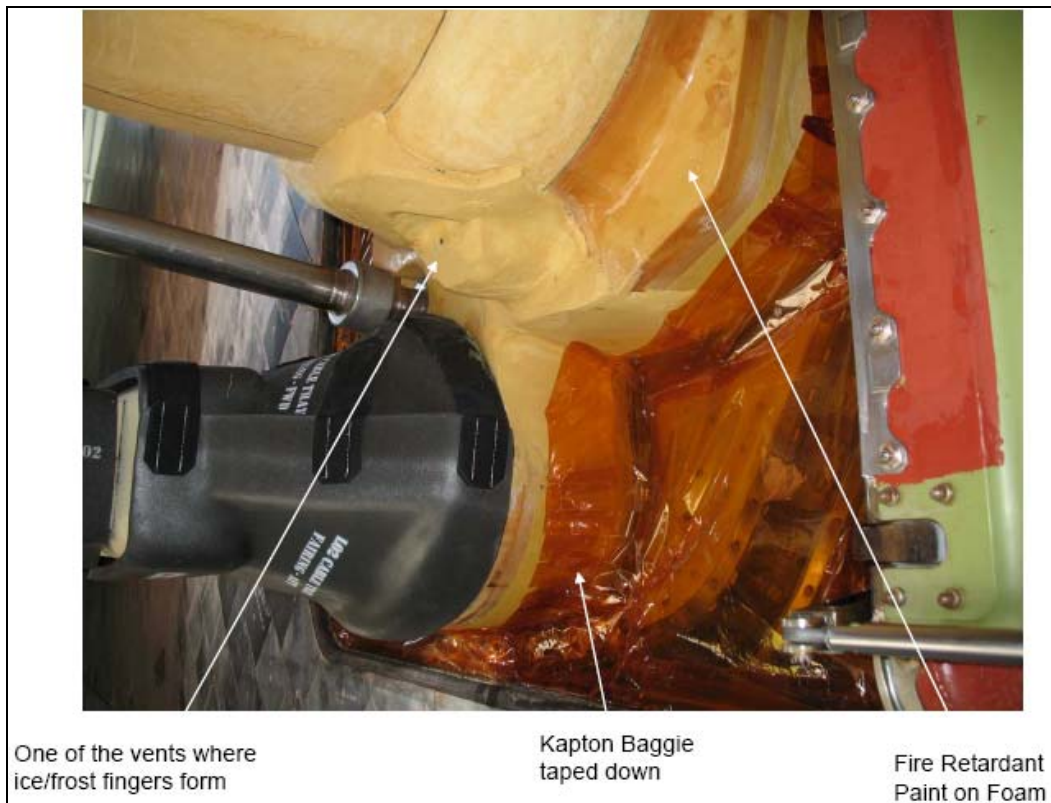


Figure 3. STS-115 LO₂ umbilical area, 23 August 2006 preflight inspection.



Figure 4. STS-115 LO₂ umbilical area access from the platform on the launch pad, 23 August 2006 preflight inspection.

Additional testing is needed to determine the optimal SILC composition, mixing and application methods, and ice adhesion performance on several substrate materials. A concern in utilizing an icephobic coating on polyurethane (PUR) or polyisocyanurate (PIR) foam is that surface degradation occurs with exposure to sunlight (UV light). An ultraviolet light absorber (UVA) incorporated into the icephobic coating can mitigate surface degradation and thus provide longer retention of the coating. Organic UVAs are known to leach out over time, so the selected UVA must have both a high UV molar absorptivity (extinction coefficient) and reactive functional groups that can bond it into the coating.

The experimental program described in this report, including 20 tests subdivided in two phases, is a follow-up to that of Ferrick et al. (2006). The double lap shear (DLS) test following ASTM D3528-96 was again used to quantify the ice adhesion performance of several related coatings and that of the optimal coating on different surfaces. Phase 1 tests focused on optimizing the ice release by and durability of the SILC coating. In phase 2, coating performance was assessed on Koropon, Kapton film, Kapton tape, and Fire-X surfaces. The adhesive performance of modified SILC containing two different weight percentages of the UVA was also evaluated in phase 2. Additional program goals were to develop protocols for reproducible and optimized coating preparation and application and to evaluate the consistency of coating performance.

2 Coating Preparation and Application

The coupon size and shape for this test program were the same as in Ferrick et al. (2006). The basic test item was again aluminum primed with Koropon. Following that initial study, two issues associated with coating preparation and application still needed resolution. The first was to develop a technique for coating application, previously consisting of spreading the material with a gloved finger. This application method was inefficient and not practical for coating large areas on the shuttle. The second issue related to preparation of the coating mixture. Mixing processes had achieved consistent results when the components did not contain volatile solvents. Unfortunately, the Rain-X mixtures that provided optimal adhesion performance contained a solvent that was rapidly lost.

To find a better application technique for the coatings, several common paint applicators were procured and assessed, including a foam roller, a float, foam brushes, a bristle brush, and a putty knife. These applicators and the resulting coatings applied to test coupons are compared in Figure 5 with that of a gloved finger. As before, the gloved finger gave a thick but even coating. The roller yielded a thick uneven layer, while the float produced a thick uneven layer and pulled the coating off the surface. The foam brush with the plastic handle resulted in a uniform thin coating with some streaking where the foam cells were located, while the foam brush with the wooden handle gave a thicker coating than the other foam brush with the same type of streaking. The bristle brush provided a uniform thick coating with bristle streaks and possible contamination from loose bristles. The putty knife gave a very uneven coating that was extremely difficult to spread. A close-up view of the coating by the foam brush with the wooden handle is also shown in Figure 5, where the improved uniformity is apparent. Based on these results, the use of a foam brush was determined to be the most effective and practical method for applying the SILC. The foam brush with the wooden handle was chosen for use, as it provided the most consistent coverage that was thick enough for application on rougher surfaces.

A standardized process using the foam brush was developed to produce a uniform, consistent, and reproducible coating. A complete, but relatively



Figure 5. Applicators being evaluated, together with their corresponding coated coupons (top), and close-up of the foam brush with wooden handle and its corresponding coated coupon (bottom).

thin coating was achieved by first applying an ample amount of SILC to both sides of the foam brush, as shown in Figure 6. Then, with one side of the brush, the SILC was applied with one stroke up; the brush was then flipped to utilize the other side, and the SILC was quickly applied with another stroke up. This process was repeated for each side of a test specimen. This application technique was used with each coating evaluated in this experimental program and for all surfaces, including Koropon, Kapton tape, adhered Kapton film, and Fire-X over Koropon.



Figure 6. Foam brush filled with SILC prior to application of the coating to the coupon surface.

Exposure of Rain-X during the weighing and mixing processes resulted in significant evaporation of volatile solvent that was variable between batches. The present study used two mixing procedures and clearly shows that larger solvent loss during preparation correlates with degraded icephobic properties of the resulting coating. The preferred preparation procedure minimizes this loss of solvent:

1. Wipe the specimen clean with isopropyl alcohol (IPA) prior to coating application.
2. Weigh out the appropriate amount of Rain-X into a mixing container.
3. Quickly add the appropriate amount of polytetrafluoroethylene (PTFE) powder into the container with the Rain-X.
4. Rapidly mix the two components with a spatula until the powder is visibly wet, but avoid over-mixing. If desired, add any additives such as a UVA to the mixture.
5. Immediately apply the mixture with a foam brush to minimize solvent evaporation. If the mixture is to be applied at a later time, then it MUST be immediately stored in an appropriately sized closed container. The mass of the wet coating applied should be about 0.02 g/cm^2 and should appear even, thin, and smooth. Brush lines are normal.
6. Allow the coating to cure for at least 24 hours prior to exposure.

3 Sample Preparation, Test, and Program Overview

Following Ferrick et al. (2006), each test specimen was a single coupon measuring 1 in. (2.5 cm) wide, 4 in. (10.2 cm) long, and 0.125 in. (0.317 cm) thick. Ice that was 0.125 in. (0.317 cm) thick adhered to the full width on two sides of the test coupon with a total initial contact area of 2.9 in.² (18.7 cm²). For consistency this ice was initially grown as strong as possible, and then subjected to temperature decreases comparable to those of the LO₂ feed line bracket. Sample preparation required a full day prior to the start of testing. Each test coupon was placed in a DLS fixture, and tape dams were applied to hold water in place during freezing. These molds were pre-cooled to $\approx 1^{\circ}\text{C}$, and pre-cooled distilled/de-ionized/de-aerated water was injected. The samples were then placed in a cold box at $-10^{\circ} \pm 0.1^{\circ}\text{C}$ ($14^{\circ} \pm 0.2^{\circ}\text{F}$) and isolated under an insulating cover to promote slower freezing. Ice growth and cool-down to the cold-box temperature occurred over 4–5 hours. Following ice growth, samples were placed in the coldroom outside the cold box and allowed to equilibrate at -16°C (3°F) for about 2 hours. Figure 7 depicts a typical set of frozen samples in the coldroom.



Figure 7. M4, M5, and control samples in the coldroom at -15°C prior to transport to the test chamber, 30 May 2006.

Three ice growth periods during 5–7 June 2006, shown in Figure 8, are typical of sample freezing in the cold box followed by coldroom temperature reduction. Sample placement in the cold box provided heat that consistently raised the temperature under the insulating cover to about -7°C (19°F). This maximum temperature was followed by an asymptotic temperature decrease over a 4-hour period, when sample freezing and equilibration at -10°C were complete. The removal of samples from the cold box was reflected by a temperature oscillation both under the cover and inside the cold box. Coldroom temperatures were not as stable as those of the cold box, continuously oscillating $\pm 1^{\circ}\text{C}$ about the mean, with periodic defrost cycles causing larger excursions.

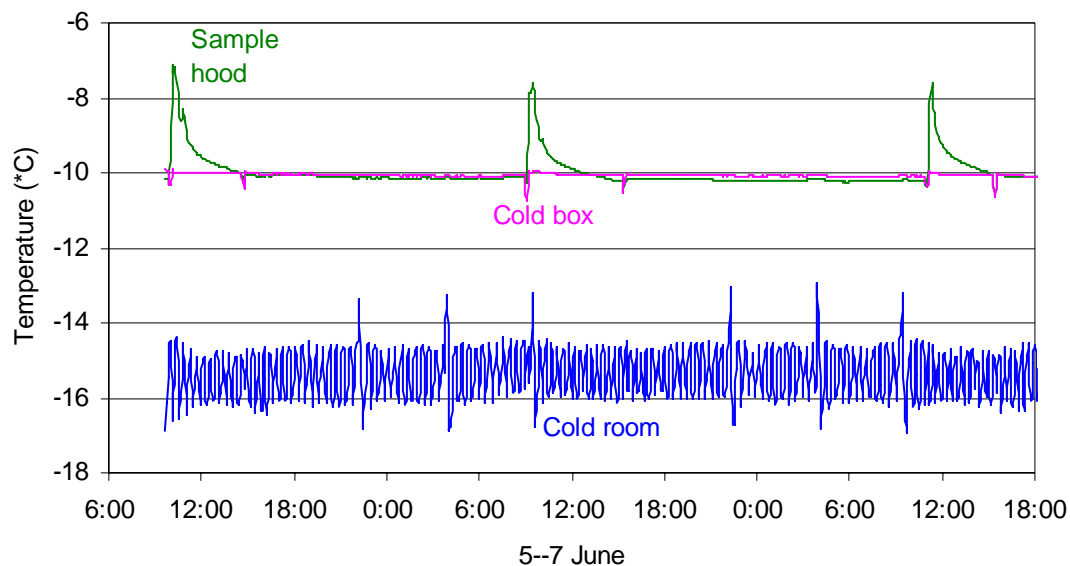


Figure 8. Temperatures under the insulated cover, in the surrounding cold box, and in the larger coldroom during growth of three sample sets, 5–7 June 2006.

Sample transport from the coldroom to the test chamber at -20°C (-4°F) followed, where constant temperature was maintained until the cool-down prior to testing. During cool-down, the test chamber temperature was decreased linearly over a period of 6 hours from -20°C to the test temperature of -112°C (-170°F), an average rate of $15.3^{\circ}\text{C}/\text{hr}$ ($28^{\circ}\text{F}/\text{hr}$). The chamber was then maintained at this temperature for 1 hour prior to testing, allowing time for the sample and chamber temperatures to equilibrate and stabilize. DLS testing was performed on an MTS machine inside the temperature-controlled chamber at -112°C (-170°F). A low and constant deformation rate of 0.005 in./min was used for about the first 10 minutes of each test, followed by a 20×-higher rate of 0.1 in./min to a total displacement of 0.5 in. and final contact area of 1.9 in.² (12.3 cm²).

Following each test the failed samples were taken to a coldroom for inspection, correlation with test data, logging of characteristics, and photographs.

The testing program had two phases. In the first phase the optimal mix of Rain-X and candidate PTFE powders was determined. The second phase tested this optimal mix on different surfaces, evaluated the effect on adhesion performance of adding different weight fractions of the UVA, and evaluated the consistency of the results through multiple test cycles.

4 Data Analysis Methods and Measures

Load data were recorded ten times per second during each test. From these data the peak load and total work were obtained, and load–displacement, load–time and displacement–time data were plotted. Peak load is an instantaneous measure that can occur at either strain rate. Conversely, total work is an integrated measure of load applied to the sample through distance. Because of the basic difference between instantaneous and integrated values, both measures provide important quantitative information concerning ice adhesion. However, these measures are not adequate to fully characterize the load–time response of a double lap shear test.

Work is directly related to strain rate, and the high strain rate segment of the test dominates the total work applied to a sample. Because of this strain rate dependence, work was recomputed as a pair of integrated values corresponding to each individual strain rate. These work measures quantify strain rate effects and are not subject to the dominance of high strain, as total work is. Another potential problem with the work measures occurs when a change in load application time between similar tests alters the work when the ice adhesion is not changed. To determine whether this problem existed and to correct for it, a pair of power measures was obtained to normalize the work at each strain rate to corresponding rates of work.

5 Phase 1 Program

Ferrick et al. (2006) found overall consistency and performance improvements of UF-8TA over MP-55 when each was mixed with Braycote. UF-8TA is an ultra-fine PTFE powder with an average agglomerated particle size of 4.0 μm , an average particle size of 0.3 μm , component particle sizes as small as 200 nm (0.2 μm), and a density of 450 g/L. Improved properties over standard PTFE include extremely good release, chemical inertness to all industrial chemicals and solvents, a wide range of service temperatures from -240 to -250°C (-400 to -482°F), low friction, and excellent non-stick properties. For comparison, MP-55 is a white, fine-particle PTFE micro-powder with an average particle size of 4.0 μm , a minimum particle size of 0.2 μm , and a density of 300 g/L. It is used as an additive in several applications, including dry film lubricants and coatings. The difference in bulk density between these powders indicates basic differences in particle size distribution. The composition of Rain-X, according to its material safety data sheet, is ethanol/SD alcohol 40, 86%; isopropanol, 4%; ethyl sulfate, 1%; polydimethylsiloxanes (silicon oil), <9%; silicic acid (H_4SiO_4), tetraethyl ester, hydrolysis products with chlorotrimethylsilane, <9%; and siloxanes and silicones, di-Me, hydroxy-terminated <9%.

Preliminary tests were conducted to determine the different weight fractions of MP-55 and UF8TA to be used for DLS testing. Results showed that MP-55 readily mixes into Rain-X at weight fractions of MP-55 ranging between 20% and 50%. On the other hand, UF8TA does not mix into Rain-X at all below about a 50% fraction. At lower fractions the UF8TA and Rain-X disassociated into two parts: PTFE and solution. The mixes that were selected for testing and corresponding abbreviations are summarized in Table 1. Mixes M5, M4, M3, M2, U57, and U5 each contained only one PTFE powder, while mix MU combined MP-55 and UF-8TA. Application of the MP-55 mixes was easier at lower fractions of PTFE. The two UF-8TA mixtures did not produce visibly complete coverage of the coated coupons. Photographs of coated M5, U5, and MU coupons are shown in Figure 9. The distinct visible difference in coatings obtained with the same method of application accurately represents the larger MP-55 and UF-8TA groups, while the MU coating is a visible compromise.

Table 1. Phase 1 coating compositions.

Group	MP-55 (% by wt)	UF-8TA (% by wt)	Rain-X (% by wt)
M5	50	--	50
M4	40	--	60
M3	30	--	70
M2	20	--	80
U57	--	57	43
U5	--	50	50
MU	30	20	50

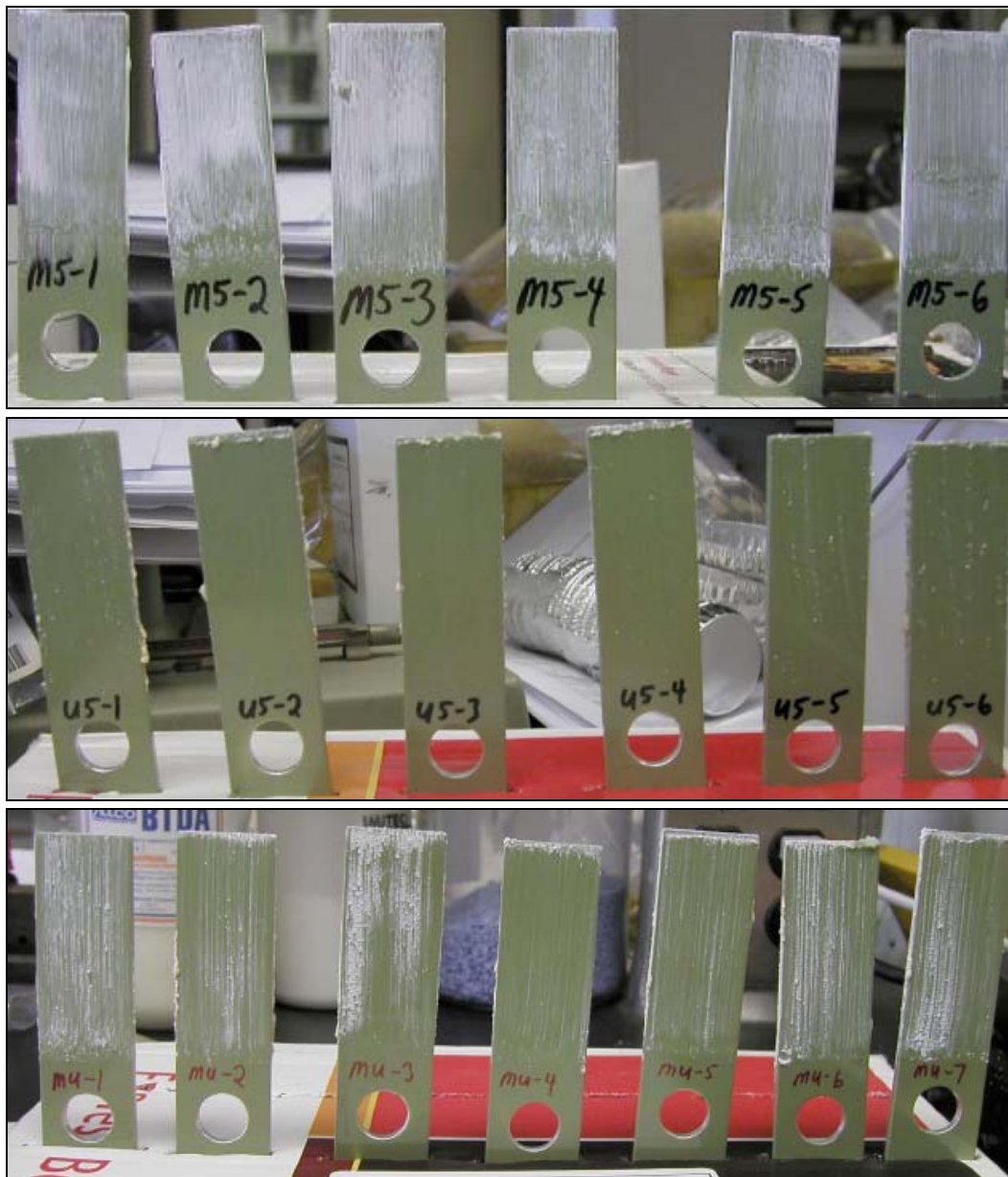


Figure 9. M5 (top), U5 (middle), and MU (bottom) coated coupons prior to phase 1 testing.

The rapid mixing procedure detailed above was used to prepare each phase 1 coating. Five test coupons were coated with each mixture, and most of these groups were tested through three cycles to determine which provided consistently optimal ice adhesion performance. The nine test series of the phase 1 program are detailed in Table 2, with the corresponding cycle noted in parentheses.

Table 2. Double lap shear test program: Phase 1.

Test	Date	Group 1	Group 2	Controls
1	31 May 06	M4 2-6(1)	M5 4-7, 9(1)	C 25, C 26
2	1 June 06	U5 1-5(1)	U57 1-5(1)	C 24, C 27
3	2 June 06	M2 1-5(1)	M3 1-5(1)	C 30, C 31
4	6 June 06	MU 1, 2, 4, 6, 7(1)	M5 4-7, 9(2)	C 32, C 33
5	7 June 06	M3 1-5(2)	M4 2-6(2)	C 34, C 35
6	8 June 06	M2 1-5(2)	MU 1, 2, 4, 6, 7(2)	C 36, C 37
7	13 June 06	M4 2-6(3)	M5 4-7, 9(3)	C 38, C 23
8	14 June 06	M2 1-5(3)	M3 1-5(3)	C 25, C 26
9	15 June 06	MU 1, 2, 4, 6, 7(3)		C 30, C 31

6 Phase 1 Results

Phase 1 sample coupons fall into three primary groups: uncoated controls, mixture variations of UF-8TA with Rain-X, and variations of MP-55 with Rain-X. The MU samples, containing both MP-55 and UF-8TA mixed with Rain-X, are included with the MP-55 variations.

Cycle 1

A pair of control samples was included in all phase 1 tests. As each coupon was thoroughly washed, rinsed with IPA, and wiped clean between re-uses, all 18 control tests will be considered as a single group. These tests were characterized by a series of audible ice fractures. The load typically increased linearly with time until a primary ice fracture occurred, greatly reducing the load. Subsequent linear load increases were also followed by fractures and sharply reduced load, producing a periodic, "sawtooth" load-time trace. The high strain rate later in the test accelerated the ice fracture processes. The amplitude of the load and the scale of the sawtooth typically diminished with increasing displacement and cumulative damage to the sample. Post-test evaluation typically revealed extensively fractured ice that remained strong enough to hold the coupon against the force applied by an observer. Residual ice adhering to the coupon after testing, termed ice collars, was common for control samples.

Cycle 1 summary data for peak load and total work are given in Table 3 for all sample groups. Corresponding average peak load and average work and power by strain rate are plotted in Figure 10. The similarity of all these adhesion measures between the controls and the U5 and U57 coated samples are evident in both the table and the figure. Figure 11 compares U57, U5, and control load-time traces of "typical" tests, each having near-average peak load and total work in their respective groups. Here again, the data are very similar. Consistent with the appearance of the UF-8TA coupons in Figure 9 (the U5 coupons in the middle photo), these data strongly suggest that very little effective PTFE was resident on the coupon surfaces. The UF-8TA variations were not significantly different from each other or from the controls, confirming chemical inertness to the solvents in Rain-X. Without additional test cycles it is clear that UF-8TA mixed with Rain-X does not provide an effective icephobic coating. Conversely, the tabulated and plotted data indicate that for the MP-55 variations,

higher MP-55 weight fractions performed best, and all groups were separated by an order of magnitude from the control, U5, and U57 data. The precise chemical and/or physical differences between the UF8TA and the MP-55 that give rise to these differences in performance have not been elucidated.

Table 3. Summary of results, Phase 1, Cycle 1.

Test Series	Peak Load (lb)				
	Mean \pm Std Dev		Median	Maximum	Minimum
M5	37	9	36	52	26
M4	38	7	37	50	31
M3	48	22	42	82	22
M2	69	24	56	110	46
MU	74	19	71	97	48
U5	688	105	670	818	533
U57	788	138	804	973	563
Control (18)	642	164	614	964	407
Test Series	Total Work (lb-in.)				
	Mean \pm Std Dev		Median	Maximum	Minimum
M5	7.3	1.1	7.8	8.5	5.5
M4	8.5	1.3	8.0	11.0	7.4
M3	9.0	3.7	8.0	15.0	4.0
M2	7.6	1.4	7.6	9.8	5.5
MU	14.4	4.7	16	20.5	8.5
U5	106	10	99	125	98
U57	104	12	102	120	85
Control (18)	122	22	123	172	84

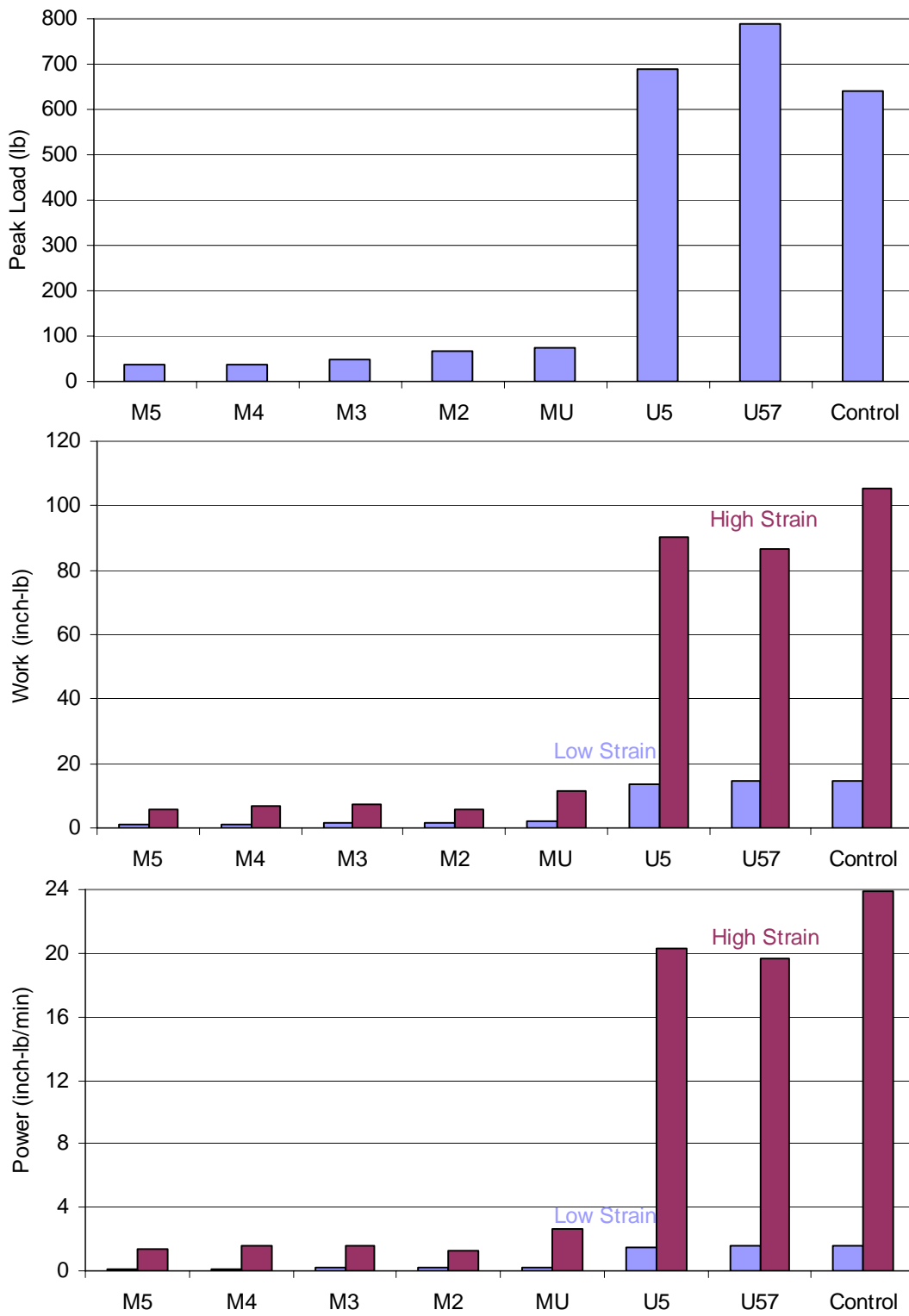


Figure 10. Phase 1 (cycle 1) results for all coupon groups: average peak load (top), average work by strain rate (middle), and average power by strain rate (bottom).

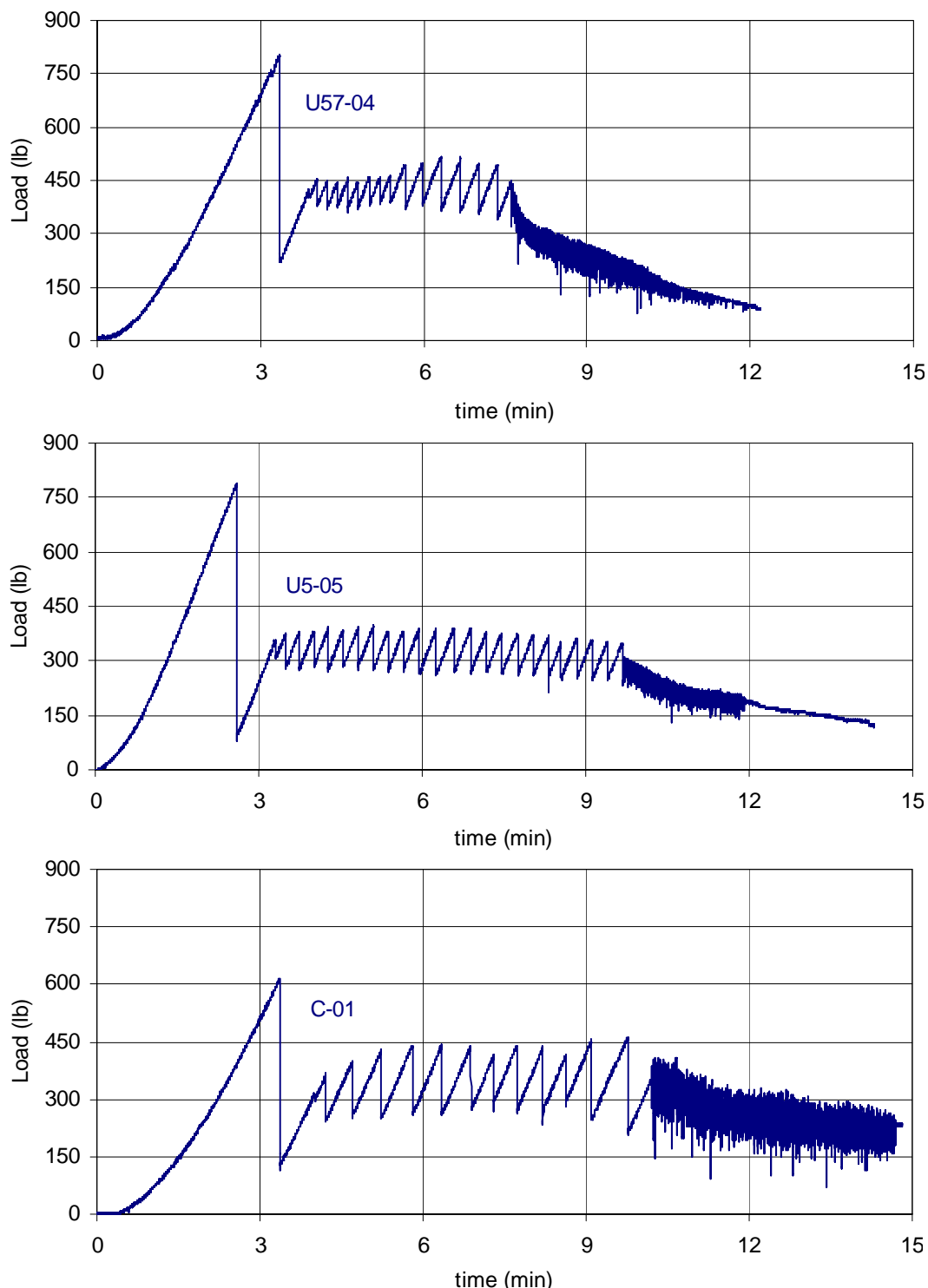


Figure 11. Phase 1 load-time traces of representative tests for the U57 coating (top), U5 coating (middle), and uncoated controls (bottom).

Cycles 2 and 3

The summary data of Table 4 indicate similar peak load and total work in cycles 2 and 3 for all MP-55 variations. In these cycles, M4 and M2 peak loads decreased, and most MP-55 variations had reduced total work relative to cycle 1, most significantly M4 and M2. Figure 12 provides peak load and work by strain rate, and Figure 13 gives power by strain rate for all MP-55 variations over the three cycles of phase 1 testing. Peak load, work and power at low strain rate, and work and power at high strain rate

Table 4. Summary of results, Phase 1, Cycles 2 and 3

Test Series	Peak Load (lb)				
	Mean \pm Std Dev	Median	Maximum	Minimum	
M5(2)	45	21	55	66	16
M5(3)	49	25	60	82	8
M4(2)	22	10	23	37	8
M4(3)	21	8	19	37	13
M3(2)	49	22	38	86	25
M3(3)	39	13	39	60	25
M2(2)	35	11	35	55	22
M2(3)	33	8	32	43	20
MU(2)	64	20	76	84	33
MU(3)	53	31	47	92	19
Test Series	Total Work (lb-in.)				
	Mean \pm Std Dev	Median	Maximum	Minimum	
M5(2)	6.6	2.6	5.8	10.0	3.0
M5(3)	5.8	2.5	5.5	8.6	1.5
M4(2)	3.2	1.3	3.8	4.2	0.7
M4(3)	2.9	0.8	2.7	4.2	1.9
M3(2)	6.6	2.6	5.9	11.5	3.9
M3(3)	5.5	3.1	3.4	10.9	2.7
M2(2)	4.4	0.8	4.2	5.6	3.3
M2(3)	3.9	0.4	4.1	4.3	3.5
MU(2)	11.5	4.7	12.0	18.5	5.7
MU(3)	12.6	7.9	11.6	24.1	3.6

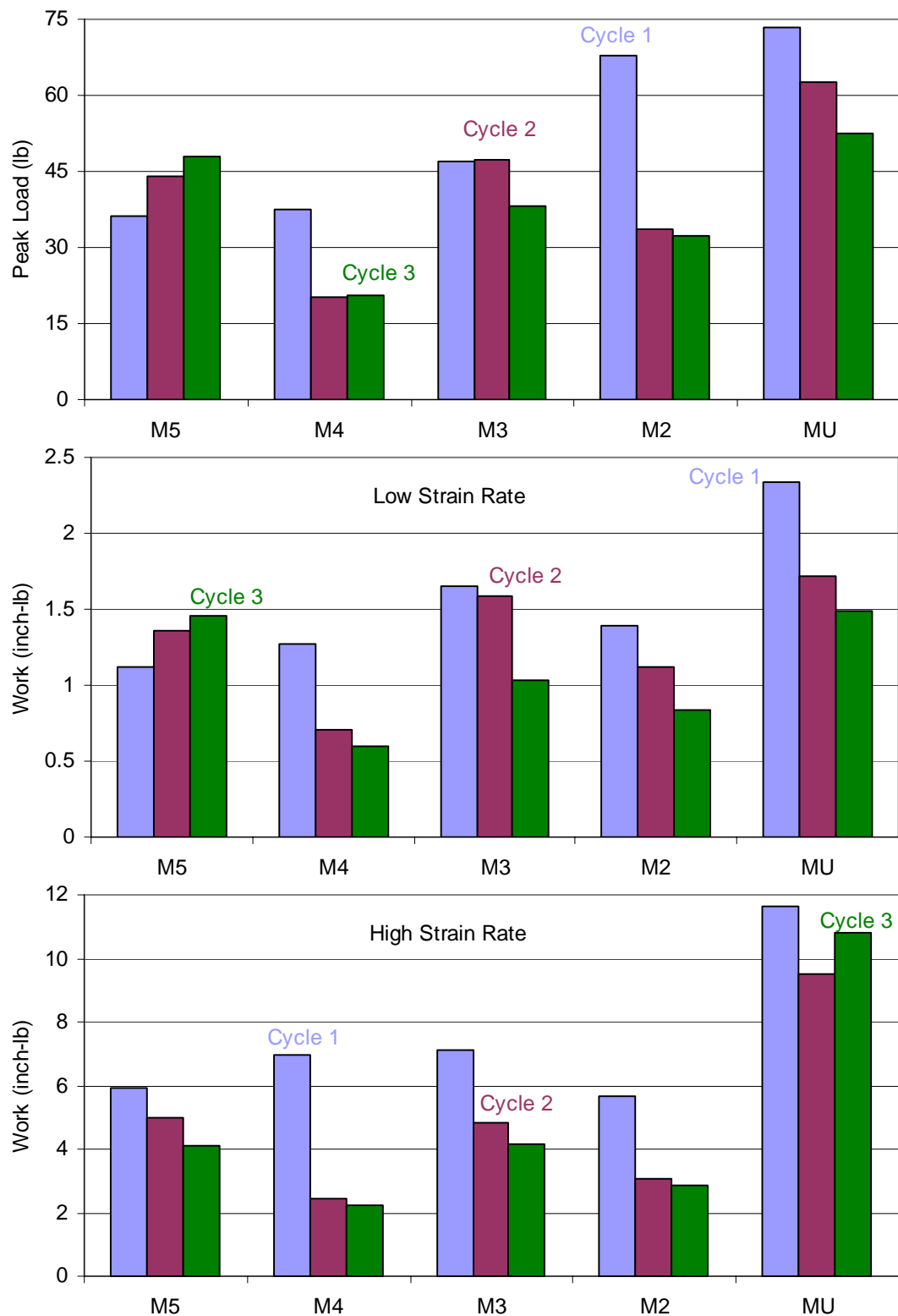


Figure 12. Average peak load (top), average work at low strain rate (middle), and average work at high strain rate (bottom) for all MP-55 coating variations over three cycles of phase 1 testing.

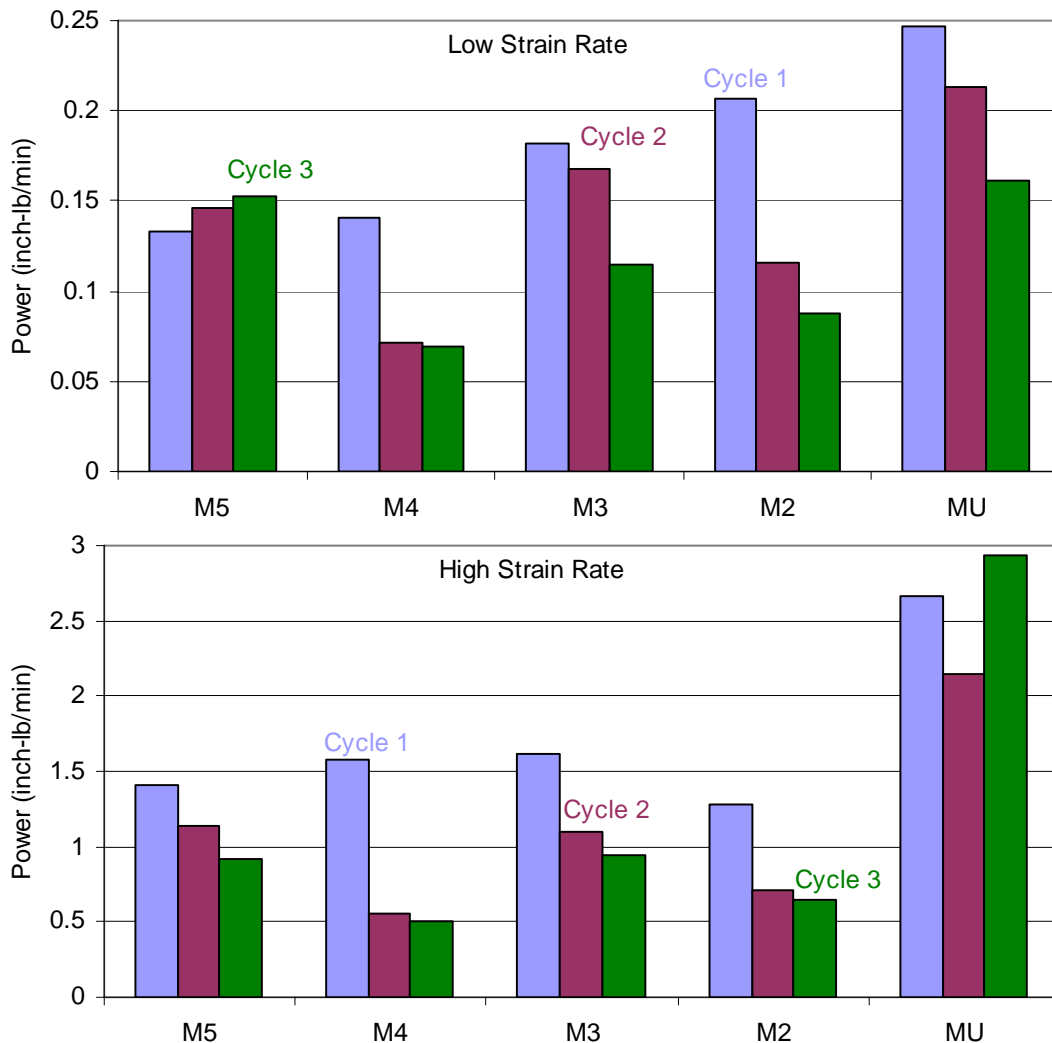


Figure 13. Average power at low strain rate (top) and at high strain rate (bottom) for all MP-55 coating variations over three cycles of phase 1 testing.

displayed similar trends through three cycles. Variations M3 and MU contained the same quantity of MP-55, but the performance measures indicate greater ice adhesion with the addition of UF-8TA, clearly favoring the M3 coating. M5 had a slight edge over the other MP-55 variations in most adhesion measures for cycle 1, while M4 was far superior when these measures are compared over three cycles. M5 and M4 peak load and total work are compared by individual coupon through three cycles in Figures 14 and 15, respectively. The peak load variability of the M5 samples increases with cycle, while the variability in M4 is essentially constant. Similarly, the total work variability of M5 samples also increases with cycle, but the M4 total work magnitude and variability decrease with cycle.

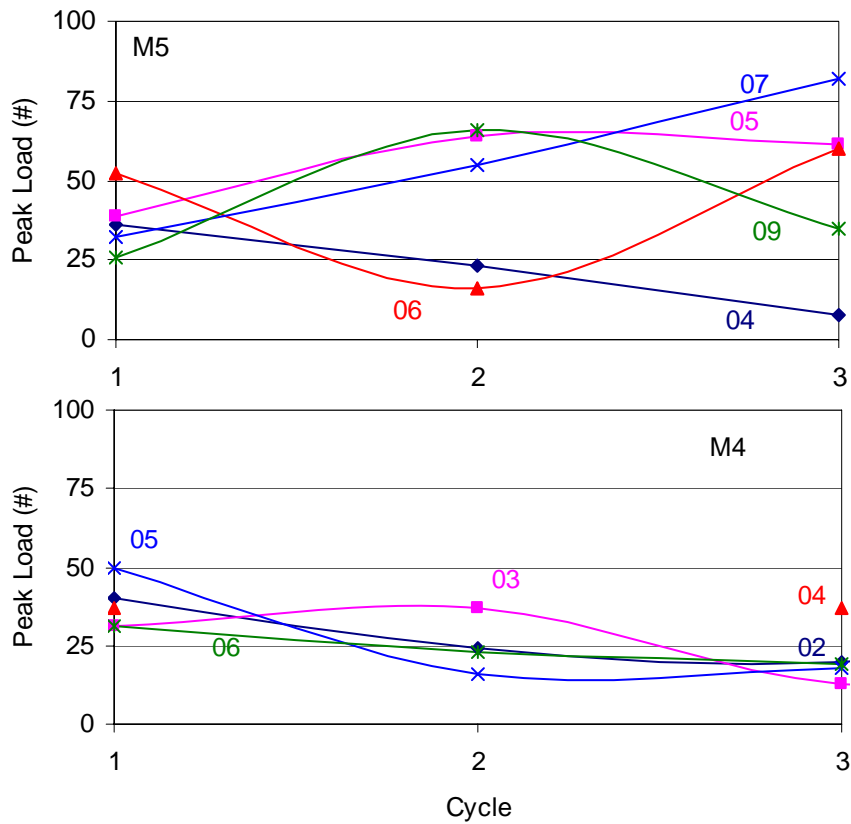


Figure 14. Peak load of individual coupons through three cycles of phase 1 testing: M5 (top) and M4 (bottom).

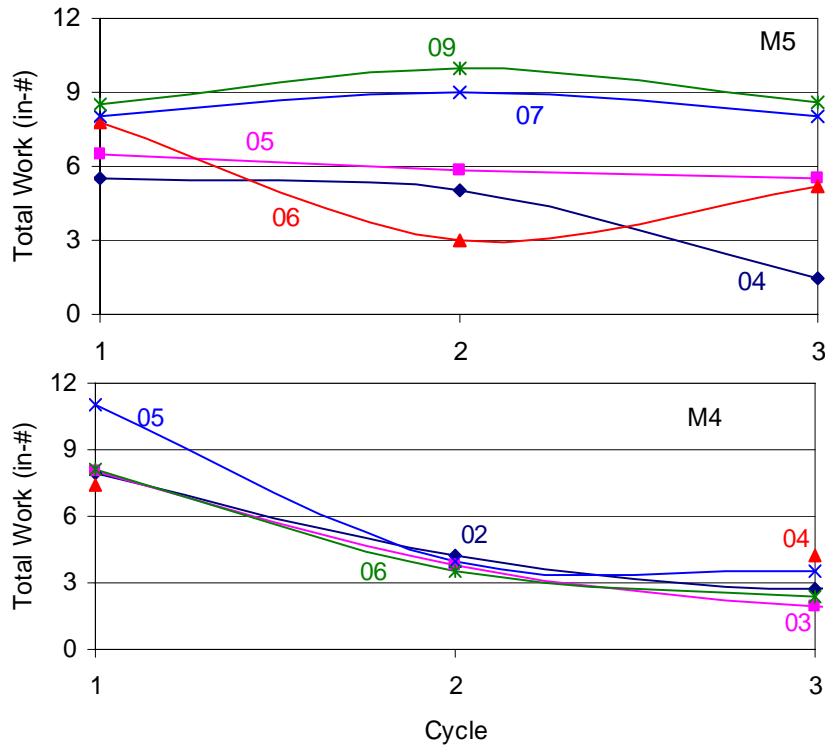


Figure 15. Total work of individual coupons through three cycles of phase 1 testing: M5 (top) and M4 (bottom).

Load–time traces for representative individual tests from cycles 1 and 3 are presented in Figure 16. For the M5 group, peak loads were generally higher in cycle 3 as shown by this comparison. The widths of the M5 cycle 1 traces were typically greater than those of cycle 3. In contrast, the M4 peak loads were generally higher in cycle 1 than in cycle 3. However, like the M5 group, the width of the M4 cycle 1 traces were greater than those of cycle 3, corresponding to decreased stick-slip with the removal of excess coating material. Diminished load in response to increased strain rate was typical for both M5 and M4 samples. Post-test analysis of these sample groups revealed smooth ice at the interface with the coupon that did not show evidence of damage from testing, and coupons moved easily by hand. Decreasing amounts of coating retained on the ice surface following each successive cycle indicate repeated failure within the coating. The progressive loss of coating from the M4 coupon surfaces is visible in Figure 17, which shows this set of samples after each test cycle.

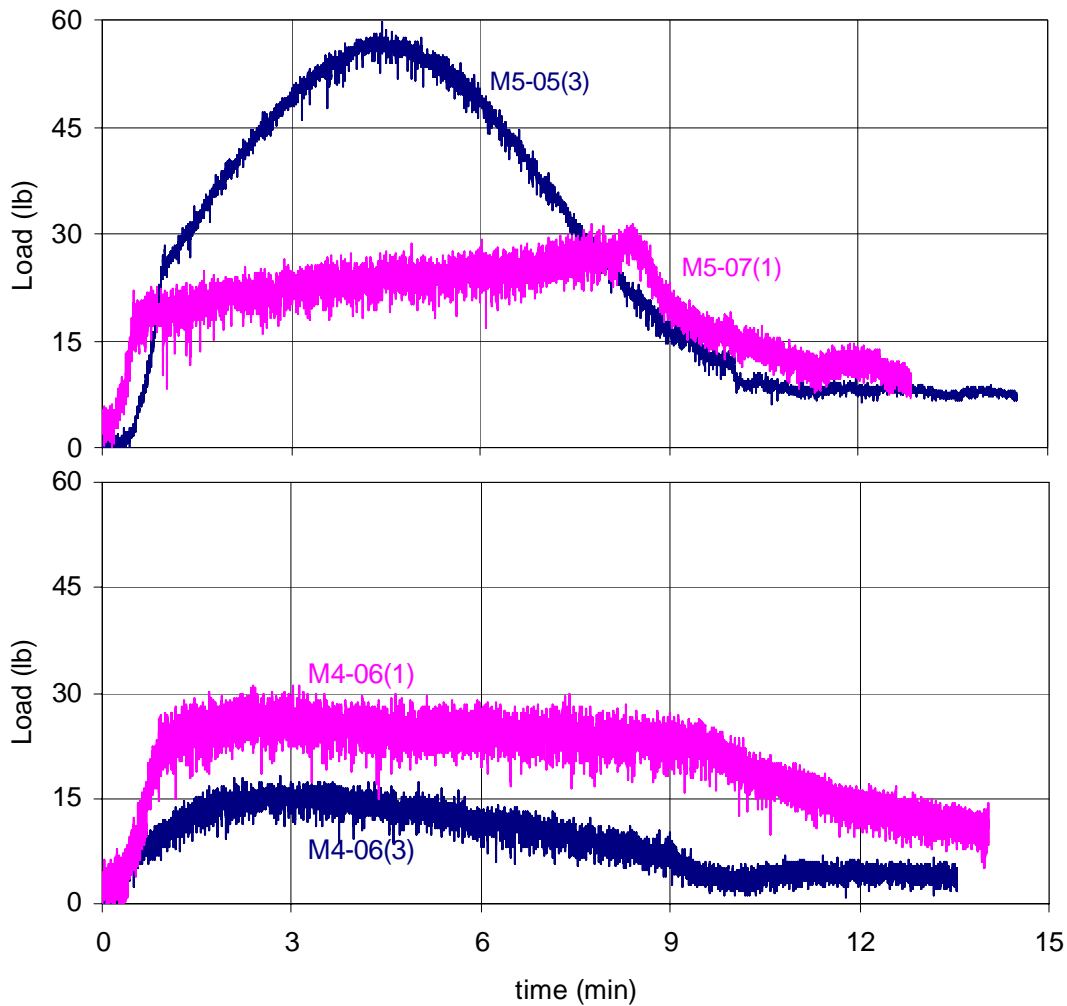


Figure 16. Comparison of representative load–time traces of cycles 1 and 3: M5 (top) and M4 (bottom).



Figure 17. M4 coupons after one (top), two (middle), and three (bottom) test cycles.

7 Phase 1 Conclusions

Performance measures used by Ferrick et al. (2006) showed reduced ice adhesion and improved consistency of UF-8TA over MP-55 when mixed with Braycote. However, the UF-8TA–Rain-X variations tested in phase 1 were not significantly different from each other or from the controls, confirming chemical inertness to the solvents in Rain-X. Also, a PTFE mixture of MP-55 and UF-8TA with Rain-X produced an increase in ice adhesion compared to a coating with the same quantity of MP-55 and no UF-8TA. These results indicate that UF-8TA mixed with Rain-X does not provide an effective icephobic coating. Consistent with the findings of Ferrick et al. (2006), the phase 1 tests verified that Rain-X mixed with MP-55 is an outstanding coating to reduce ice adhesion to Koropon-primed aluminum at cryogenic temperatures. Significant but decreasing amounts of coating were retained on the ice following each successive test cycle, indicating repeated failure in the coating. The precise chemical and/or physical differences between UF8TA and MP-55 that give rise to performance differences have not been elucidated. The ice adhesion performance measures for three cycles of phase 1 testing showed that the M4 mix was best and most consistent by a wide margin over all other mixes. As a result, M4 was selected as the basis of all phase 2 mixes.

8 Phase 2 Program

Three coating variations of M4 were tested in phase 2, along with application of the basic coating to four different surfaces. Coated coupons were generally tested in groups of five through either two or four cycles. In addition, three coupons from the M4 group of phase 1 were tested through cycles 4 and 5 in phase 2.

Phase 2 coatings were M42, a remake of the optimal M4 phase 1 mix, and two related mixes with the same 60:40 Rain-X to MP-55 weight ratio that contained the UVA. Mix MT was 55% Rain-X, 37% MP-55, and 8% UVA by weight, and mix MT4 had 58% Rain-X, 38% MP-55, and 4% UVA. In contrast to M4, the M42, MT, and MT4 coatings were mixed identically using the thorough but slow procedure detailed in Ferrick et al. (2006). Surfaces tested in phase 2 included standard Koropon-primed aluminum, Kapton film (K), Kapton tape (KT), and Fire-X (F) over Koropon-primed aluminum. The rapid mixing procedure detailed above in this report was used to prepare the coating for the K, KT, and F coupon groups.

The objectives of this program were to verify the ice adhesion effectiveness and durability of the optimal coating for several surfaces of potential application on the shuttle and to quantify any change in effectiveness resulting from the addition of the UVA to the mix. The eleven tests of the phase 2 program are detailed in Table 5, where cycle number is again in parentheses.

Table 5. Double lap shear test program: Phase 2.

Test	Date	Group 1	Group 2	Controls
10	20 June 06	KT 1-3 (uncoated)	M4 3,6(4), M5 4(4)	C 32, C 33
11	21 June 06	K 1-4 (uncoated)	M42 1-4(1), MT 1-4(1)	C 34, C 35
12	22 June 06	KT 4-8 (uncoated)	KT 9-13(1)	C 36, C 37
13	27 June 06	M42 1-4(2), M42 5(1)	MT 1-4(2), MT 5(1)	C 38, C 23
14	28 June 06	F 1-5 (uncoated)	F 6-10(1)	C 25, C 26
15	29 June 06	K 5-9(1)	M42 5(2), MT 5(2), M4 3,6(5), M4 2(4)	C 30, C 31
16	12 July 06	MT4 1-5(1)	K 1-4, 11 (uncoated), M4 2(5)	C 32, C 33
17	13 July 06	MT 1-5(3)	M42 1-5(3)	C 34, C 35
18	14 July 06	KT 9-13(2)	K 5-9(2)	C 36, C 37
19	18 July 06	F 6-10(2)	MT4 1-5(2)	C 38, C 23
20	19 July 06	M42 1-5(4)	MT 1-5(4)	C 25, C 26

9 Phase 2 Results

Multiple Surfaces: Uncoated and Cycle 1 Coated

Peak load and total work for cycle 1 testing of Koropon (Control), Kapton tape (KT), Kapton film (K), and Fire-X (F) coupons, both coated and uncoated, are given in Table 6. Each summary record in this table represents five tests, except when a different test total is indicated by a number in parentheses. Of the uncoated coupons, F developed the greatest peak loads and total work, while KT developed the smallest. However, KT ice adhesion loads were limited by both tape and adhesive failures (Fig. 18), causing underestimated results. For all coated surfaces the peak load and work were only a small fraction of the uncoated values, demonstrating the general effectiveness of the coating. This same result can be seen more readily in Figure 19, where average peak load and average work at low strain rate and at high strain rate are compared for the coated and



Figure 18. Failed Kapton tape and adhesive resulting from uncoated DLS testing.

Table 6. Summary of results, Phase 2, Cycle 1.

Test Series	Peak Load (lb)				
	Mean ± Std Dev		Median	Maximum	Minimum
M4 (phase 1)	38	7	37	50	31
M42	79	30	68	132	47
MT	153	64	153	234	73
MT4	133	77	114	225	49
KT uncoated	284*	104	245	538	194
KT	52	24	56	91	26
K uncoated	663	108	666	913	539
K	120	20	118	157	100
F uncoated	1415	89	1379	1521	1286
F	90	43	78	173	49
F (4)	69	13	71.5	83	49
Control (22)	765	205	784	1257	480
Test Series	Total Work (lb-in.)				
	Mean ± Std Dev		Median	Maximum	Minimum
M4 (phase 1)	8.5	1.3	8.0	11.0	7.4
M42	14.1	3.6	12.2	19.8	10.9
MT	14.2	3.6	14.2	19.0	9.5
MT4	15.8	6.6	11.7	26.7	9.2
KT uncoated	78.2*	20.7	68.6	117	57.0
KT	15.6	9.0	15.2	32.1	6.1
K uncoated	193	16	195	210	162
K	49.9	10.6	50.7	66.9	37.3
F uncoated	170	20	166	198	144
F	18.3	6.3	15.7	30.2	12.4
F (4)	15.4	2.4	15.1	19.0	12.4
Control (22)	132	26	137	182	90.3

* Tape torn, substrate failure.

uncoated surfaces. Uncoated Koropon and Kapton film had similar peak loads and work at low strain rates, with Kapton tape lower and fire retardant paint higher. The large relative work at high strain rates, for both coated and uncoated Kapton film samples, breaks this pattern.

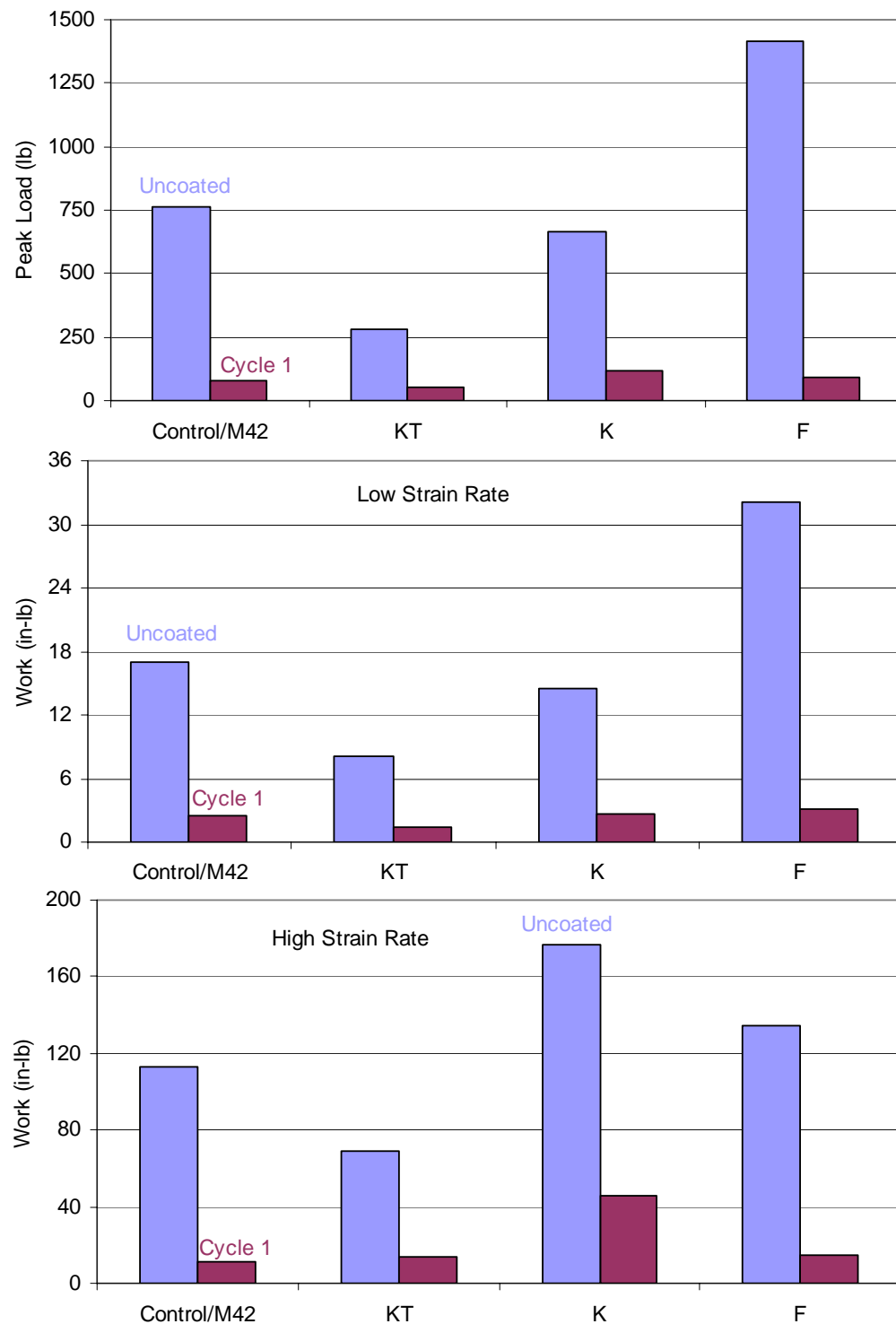


Figure 19. Comparison of average measures for uncoated and cycle 1 coated Koropon (Control/M42), Kapton tape (KT), Kapton film (K), and Fire-X (F) surfaces: peak load (top), work at low strain rate (middle), and work at high strain rate (bottom).

Figure 20 presents representative load–displacement traces of two control tests and two uncoated Kapton tests. The high strain rate portion of each test corresponds to displacements greater than 0.05 inches. In both Kapton tests the load remained high at large displacements while the control test loads diminished, and load variability at the high strain rate was also much greater than for the controls. The Kapton film had a slightly non-planar surface due to variations in the thickness of the adhesive bonding the film to the coupon and corresponding non-planar ice growth. The ice and film surfaces were matched at small deformations but not at the large deformations associated with the high strain rate. This topographic mismatch may have caused increased loads and load variability relative to that of perfectly planar surfaces.

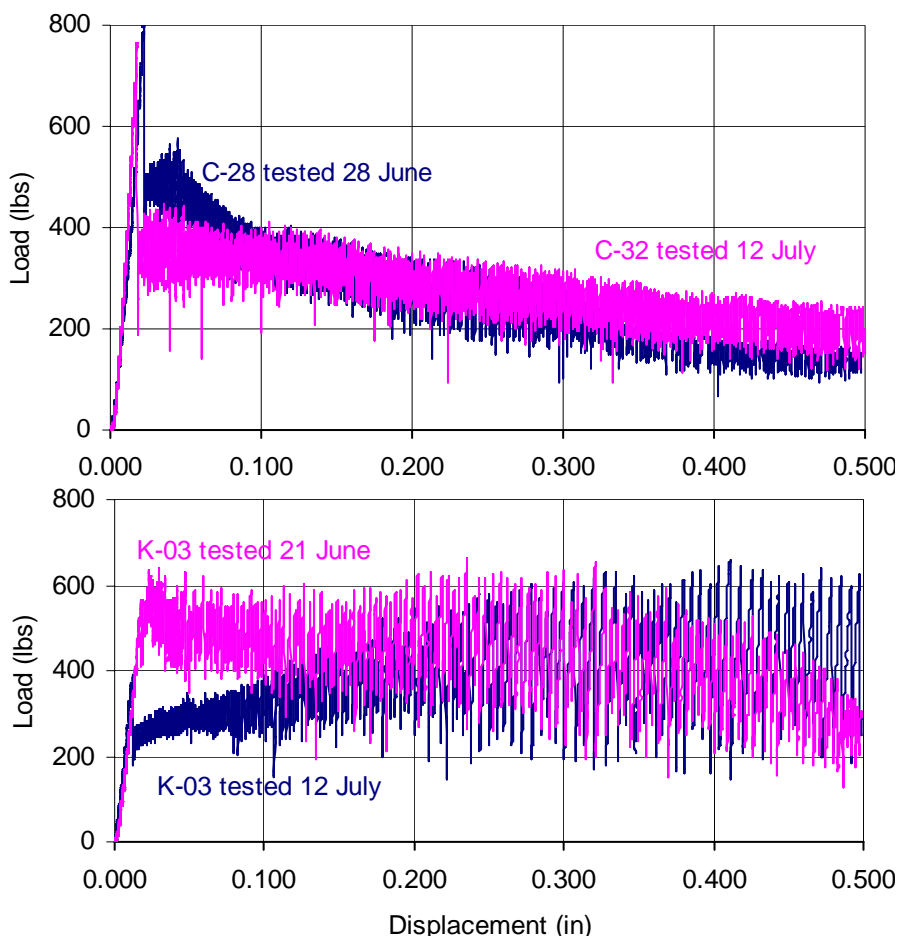


Figure 20. Load–displacement traces for representative uncoated control tests (top) and Kapton film tests (bottom). The load decrease with displacement from 0.05 to 0.5 in., the high strain rate portion, is more pronounced for the C-tests than for the K-tests.

Other significant results relating to coating preparation and modification are also contained in Table 6. The mean and median peak loads doubled between the cycle 1 M4 (phase 1) and M42 (phase 2) test series.

Corresponding differences in total work were also large. These two coatings used the same recipe and were applied to the coupons in the same manner with a foam brush. The primary difference between the batches was in the extent of mixing during coating preparation. The M4 preparation included minimal mixing, just enough for the Rain-X to completely wet the MP-55. The M42 preparation included extended mixing of the two components with several hundred strokes. Because components of Rain-X are volatile, extended mixing allows time for significant solvent losses to occur, an apparent cause of degraded ice adhesion performance.

The effect of the addition of the UVA on cycle 1 adhesion performance of the SILC mix can be seen by comparing MT (8% UVA) and MT4 (4% UVA) with M42 in Table 6. The peak loads developed by both UVA mixes are higher than those of M42, but total work was essentially unchanged.

Load-time traces for tests that are typical of each series are compared in Figure 21. An initial high peak load was typical of both UVA coatings, occurring in four of the five tests of each. Following this peak, the loads decreased sharply and became similar to those of M42 over the remainder of the test. The cycle 1 results indicate that the extent of mixing during coating preparation may have a comparable or greater effect on ice adhesion to the SILC than the addition of UVA. However, corroborating data from higher test cycles are needed to confirm this observation.

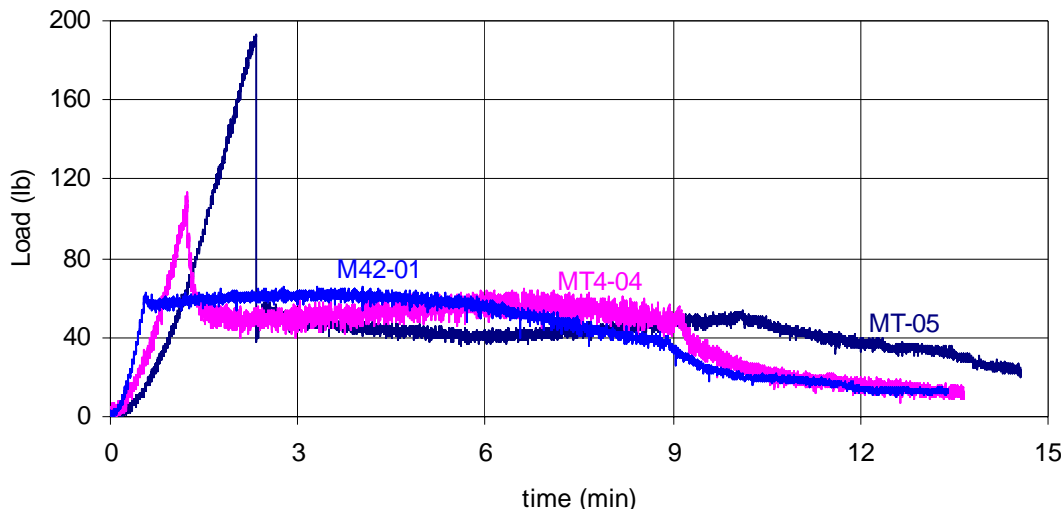


Figure 21. Load-time traces of representative M42, MT, and MT4 tests in cycle 1.

Multiple Surfaces and Higher Cycle Coated

The results of cycle 2 tests are summarized in Table 7. Peak load and total work for the M42 coating on the various surfaces were comparable in cycle 2 to those of cycle 1. The factor-of-three differences in mean and median peak load and total work between M4 (phase 1) and M42 (phase 2) in cycle 2 are even larger than those of cycle 1. The MT and MT4 coatings also outperformed M42 in peak load and total work for cycle 2. Representative load-time traces for M42, MT, and MT4 in cycle 2 are presented in Figure 22. The initial peak of the MT cycle 1 trace was greatly reduced in amplitude in cycle 2 and did not provide the overall peak in any test. The initial peak of the MT4 cycle 1 tests was absent in all cycle 2 tests. These data provide additional support for the conclusion that over-mixing during coating preparation has a greater effect on ice adhesion to the SILC than the addition of the UVA. These remarkably similar cycle 2 load traces also

Table 7. Summary of results, Phase 2, Cycle 2.

Test Series	Peak Load (lb)				
	Mean \pm Std Dev	Median	Maximum	Minimum	
M4 (phase 1)	25	8	24	37	16
M42	95	41	77	164	61
MT	68	20	61	107	53
MT4	65	15	67	81	43
KT	34	10	35	46	20
K	135	29	125	191	106
F	64	24	57	110	40
F (4)	53	8	56	59	40
Test Series	Total Work (lb-in.)				
	Mean \pm Std Dev	Median	Maximum	Minimum	
M4 (phase 1)	3.9	0.3	3.9	4.2	3.5
M42	16.6	6.3	14.0	27.1	11.4
MT	11.2	3.2	9.5	15.5	7.2
MT4	8.3	2.4	8.4	12.4	5.4
KT	8.3	2.6	8.3	11.9	4.6
K	53.6	13.8	48.0	80.4	43.4
F	14.2	4.1	14.4	21.2	10.1
F (4)	12.5	2.5	12.3	15.3	10.1

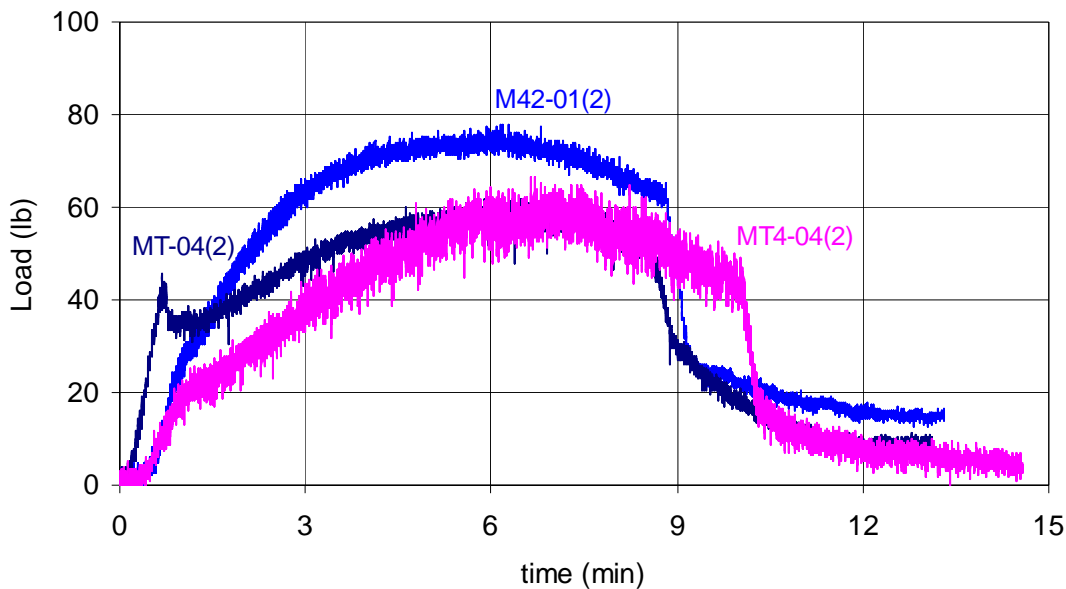


Figure 22. Load–time traces of representative M42, MT, and MT4 tests in cycle 2.

imply that residual solvent within the UVA was largely removed from the MT4 and MT coupons after the first cycle. Supplemental analysis of tested MT4 and MT coupons for changes in the coating is recommended, as other phenomena could also cause the enhanced coating performance.

Peak load and work at low and high strain rates are compared in Figure 23 for the various coated surfaces during cycles 1 and 2. Coated KT and F improved slightly in all measures between cycles 1 and 2, while coated K and Koropon surfaces had measures that were comparable or slightly increased in cycle 2. In both cycles K had the highest peak loads and by far the highest work at the high strain rate. Both load–time and load–displacement traces were very similar for the individual K coupons in each cycle. Test groups K, KT, F, and MT4 are pictured in Figure 24 after two cycles. All of these coupons retained significant coating, but the K group displayed linear abrasions of the coating that were not evident in the other groups. The sum of this evidence supports the earlier conclusion that the ice–Kapton film topographic mismatch caused overestimated peak loads and work at high strain rate for both coated and uncoated samples.

M42 and MT coupons were tested through four cycles. Phase 2 testing also included cycles 4 and 5 for three M4 coupons. Of these, M4 sample 06 was damaged during cycle 4 handling, and data for that coupon/cycle were not obtained. A summary of results for peak load and total work in cycles 3–5 is given in Table 8. In cycles 3 and 4, M42 had higher peak loads but lower total work than MT, indicating the absence of the MT peak that was typical

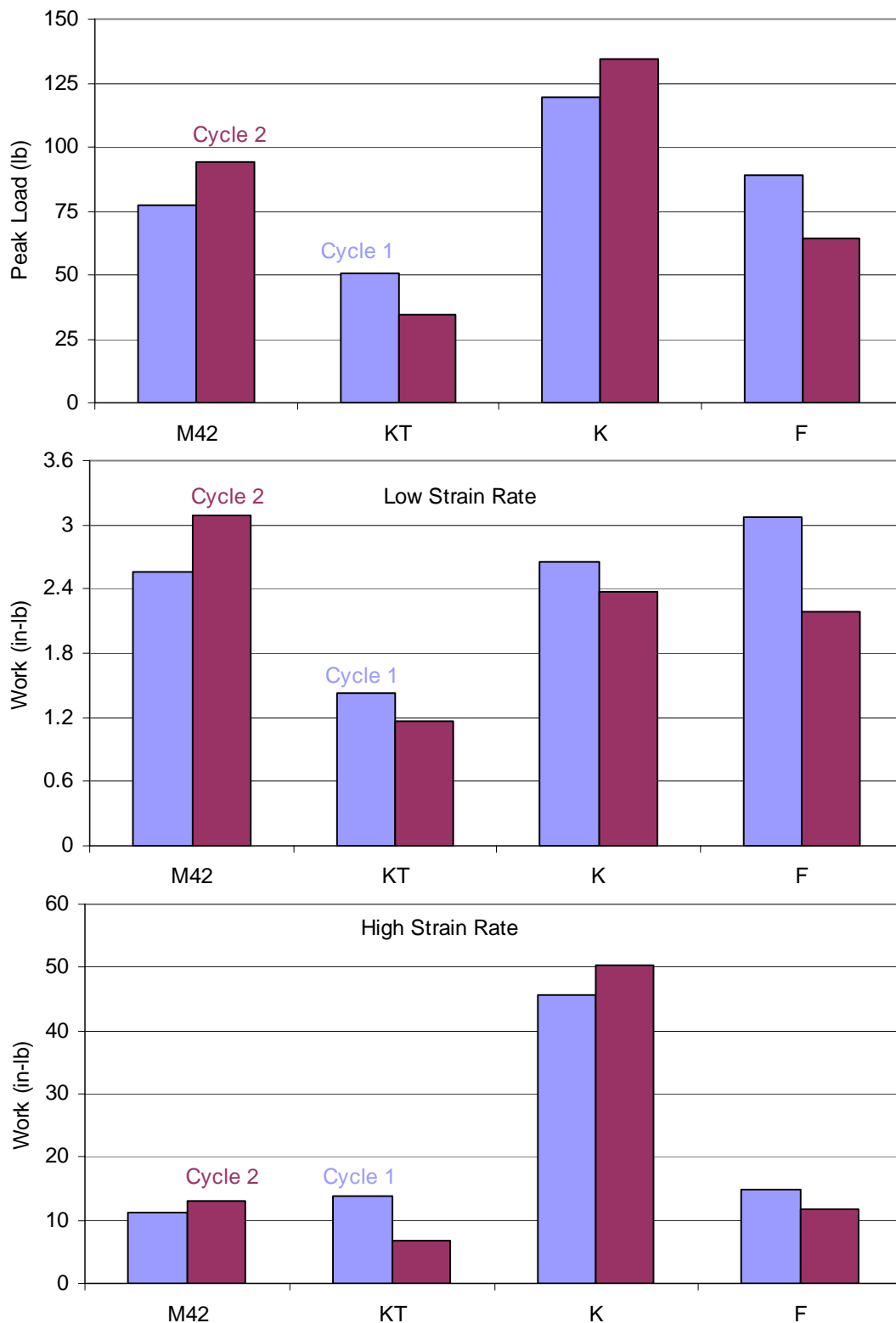


Figure 23. Average measures through two cycles for SILC applied to Koropon (M42), Kapton tape (KT), Kapton film (K), and Fire-X (F) surfaces: peak load (top), work at low strain rate (middle), and work at high strain rate (bottom).



Figure 24. Coated Kapton film and Kapton tape after two test cycles (top), Fire-X and MT4 after two test cycles (middle), and MT and M42 after four test cycles (bottom).

of cycle 1 and comparable performance overall. Corresponding measures for M4 in these cycles improved on those of the better phase 2 coating by more than a factor of 2. Consistent with the appearance of other SILC variations, Figure 24 shows minimal visible coating remaining on the test area toward the top of the M42 and MT coupons after cycle 4.

Table 8. Summary of results, Phase 2, Cycles 3, 4, and 5.

Test Series	Peak Load (lb)				
	Mean \pm Std Dev	Median	Maximum	Minimum	
Cycle 3					
M4 (phase 1)	21	8	19	37	13
M42	58	24	65	82	14
MT	54	17	50	85	36
Cycle 4					
M4	27	9	27	36	18
M42	75	26	85	107	34
MT	62	21	57	91	38
Cycle 5					
M4	17	5	16	24	12
Test Series	Total Work (lb-in.)				
	Mean \pm Std Dev	Median	Maximum	Minimum	
Cycle 3					
M4 (phase 1)	2.9	0.8	2.7	4.2	1.9
M42	8.3	3.5	8.6	13.3	2.6
MT	10.8	2.2	10.3	14.8	7.9
Cycle 4					
M4	3.2	1.6	3.2	4.7	1.6
M42	11.0	3.6	10.0	16.2	5.6
MT	17.2	5.2	15.3	25.6	12.7
Cycle 5					
M4	2.9	0.8	3.4	3.6	1.8

Figure 25 compares peak load and work at low and high strain rates for M4, M42, MT, and MT4 for up to four test cycles. MT and MT4 samples developed greater peak loads in cycle 1 relative to M42, but these peak loads were comparable or lower in the higher test cycles. Work at low strain rate was consistently greater for M42 relative to MT through four cycles. MT4 developed greater work at low strain rate than MT in cycle 1 but was comparable in cycle 2. M42, MT, and MT4 developed comparable work at high strain rate through the test cycles. Individual M4 coupon peak load and total work through five cycles are presented in Figure 26. These data show relatively high peak loads and total work in cycle 1,

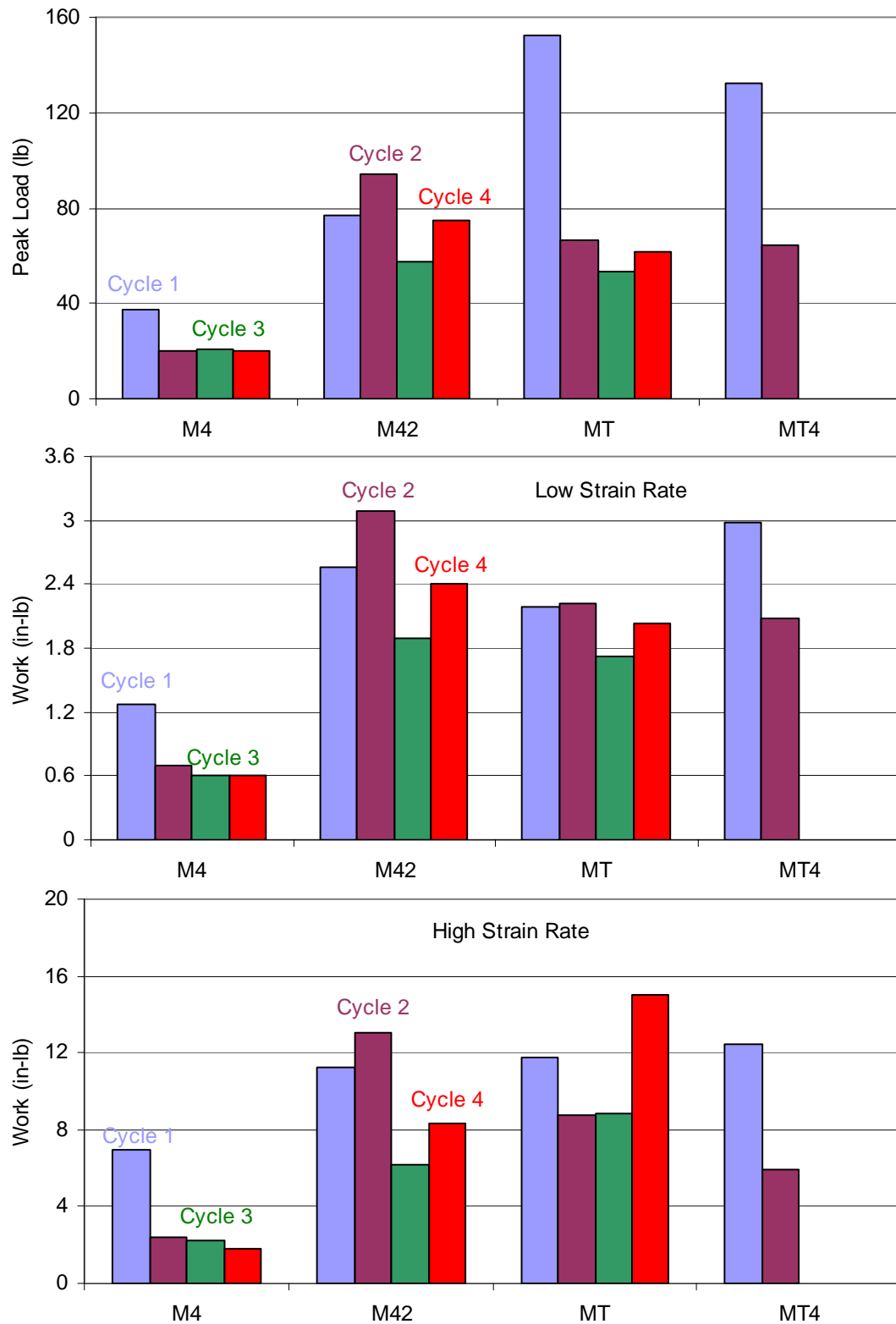


Figure 25. Average measures through two or four test cycles comparing M4, M42, MT, and MT4 coatings: peak load (top), work at low strain rate (middle), and work at high strain rate (bottom).

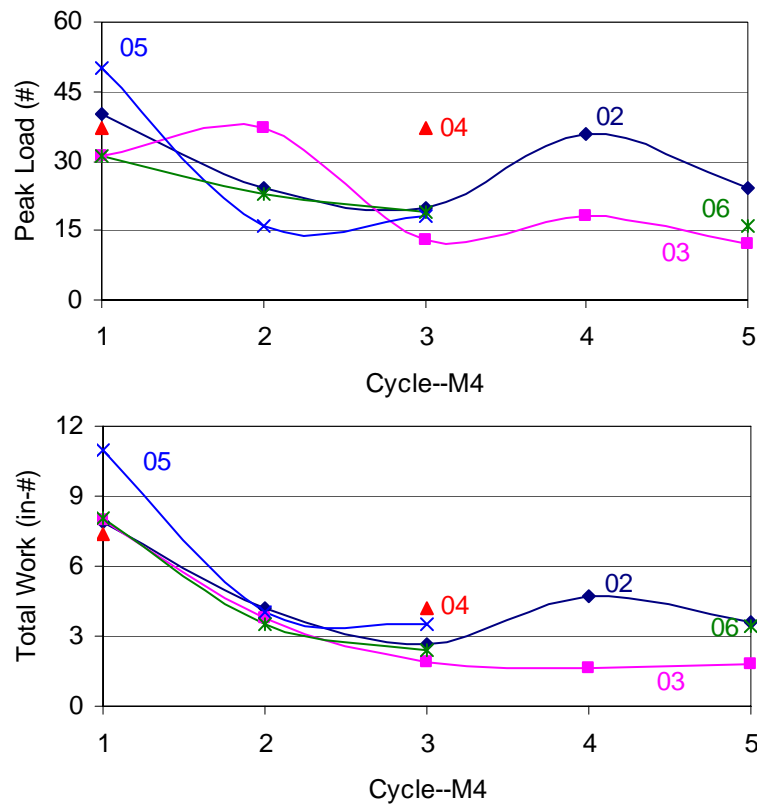


Figure 26. Peak load (top) and total work (bottom) of individual M4 coupons through five test cycles.

followed by consistent values and variability of these measures in cycles 2–5. M4-06 was the most representative of the tests conducted in cycles 3 and 5, and these load–time traces are compared in Figure 27 at a greatly expanded scale. The shapes of these traces are slightly different, but all

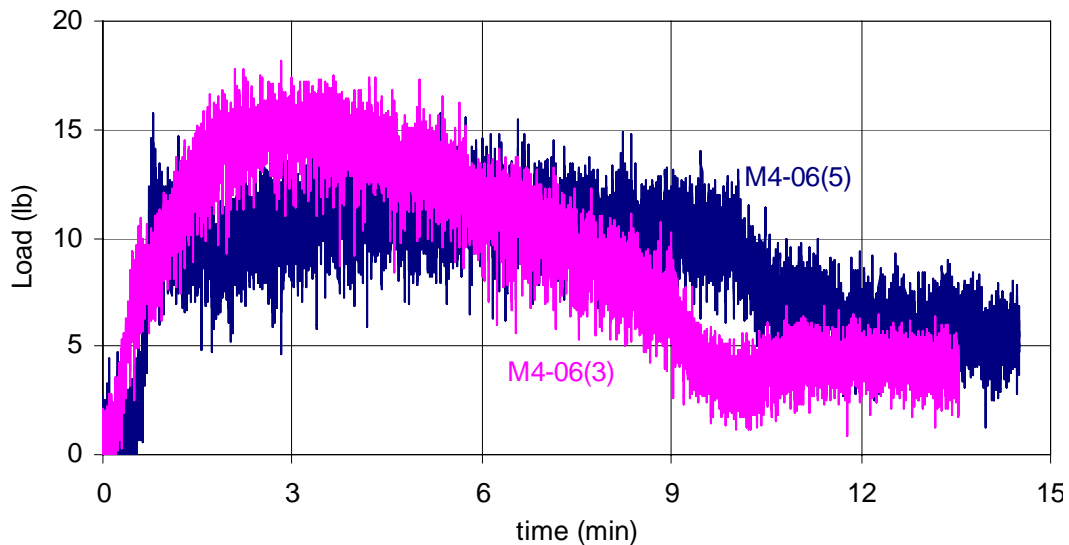


Figure 27. Comparison of representative M4 load-time traces for cycles 3 and 5. The cycle 3 trace is re-plotted from Figure 16 at an expanded scale.

measures are essentially the same. Cycle 5 ice adhesion measures for M4 were as good as or better than those of any previous cycle, demonstrating outstanding coating durability. Overall, the M4 measures clearly show that it was the outstanding performer of this group of coatings.

During individual tests in all cycles the load generally decreased with the increase in strain rate. Post-test analysis of the phase 2 mixes that followed each cycle revealed smooth planar ice surfaces at the interface with the coupon, some fracturing of the ice, and a diminishing quantity of coating material retained both on the coupons and on the ice with each successive test cycle. Post-test analysis for M4 cycles 4 and 5 showed no evidence of ice fracture initiated at the planar interface with the coupon, and only small quantities of visible coating material were retained on the ice surfaces. These results verify both the performance and durability of the optimal coating through five cycles of ice growth and adhesive failure.

10 Phase 2 Conclusions

The measurements for the coated coupons with Koropon (M42), Kapton tape (KT), Kapton film (K), and Fire-X (F) surfaces were only a small fraction of the corresponding values for uncoated coupons, demonstrating the general effectiveness of the SILC. The only loss of ice adhesion performance caused by the UVA was the high initial peak load of cycle 1. The load traces of the MT, MT4, and M42 groups were remarkably similar in cycle 2 and higher, implying that the solvent within the UVA may have been largely removed from the MT and MT4 coupons in the first cycle. Supplemental analysis of tested MT and MT4 coupons for differences within the coatings is needed to confirm this hypothesis. Over-mixing during coating preparation caused a greater increase in ice adhesion to the SILC than that of adding the UVA to the mixture. Phase 2 results also verified the sustained peak performance and durability of M4 as the optimum coating through five cycles of ice growth and adhesive failure.

11 Ice Structure and Fracturing during Cryogenic DLS Testing

Ice fracture occurs from induced thermal stresses during cooling in the test chamber to cryogenic temperatures, prior to any load application in DLS testing. Additional ice fractures are induced during DLS testing of samples that are not effectively coated. This study was designed to determine whether the differences in fracturing are visible between ice specimens as grown and ice specimens that have been cooled to -112°C and tested, both with and without an effective coating.

Selected ice samples were removed from the DLS molds and mounted on glass slides, and thin sections were prepared on a microtome for each of the three conditions. Ice sample NC was grown on 18 July 2006 using the standard procedure and was removed from the mold without cryogenic cooling or DLS testing. DLS sample M4-2(5) was a coated sample tested on 12 July 2006 that developed a peak load of 24 lb and total work of 3.6 in.-lb. Very little coating remained on the ice following this cycle 5 test, making it a good specimen for analysis. Uncoated Kapton samples (K) were also tested on 12 July, with peak loads between 661 and 689 lb and total work between 190 and 210 in.-lb. The objectives of this analysis were to observe, photograph, and compare the air bubbles, ice fractures, and crystalline structures for these conditions.

General backlighting and cross-polarized light photographs of the NC samples, obtained from the two sides of a single mold, are given in Figure 28. There are many air bubbles in the samples, and the bubble distribution seems to be influenced by the ridges in the DLS mold. No ice fractures are evident in sample NC, and the crystal structure is fine grained and complex, with one side of the mold displaying larger crystals than the other. Studies have shown that fine-grained ice is significantly stronger in mechanical testing than course-grained ice. Differences in bubble concentration and grain size may favor fracture development in different locations on the two sides of a single sample and between samples. Corresponding photographs for the two sides of coated sample M4-2(5) are given in Figure 29. Ice fractures are evident in the backlit photograph, and again, the ice has a complex, fine-grained structure with a range of grain sizes. Finally, Figure 30 presents photographs of uncoated K-sample

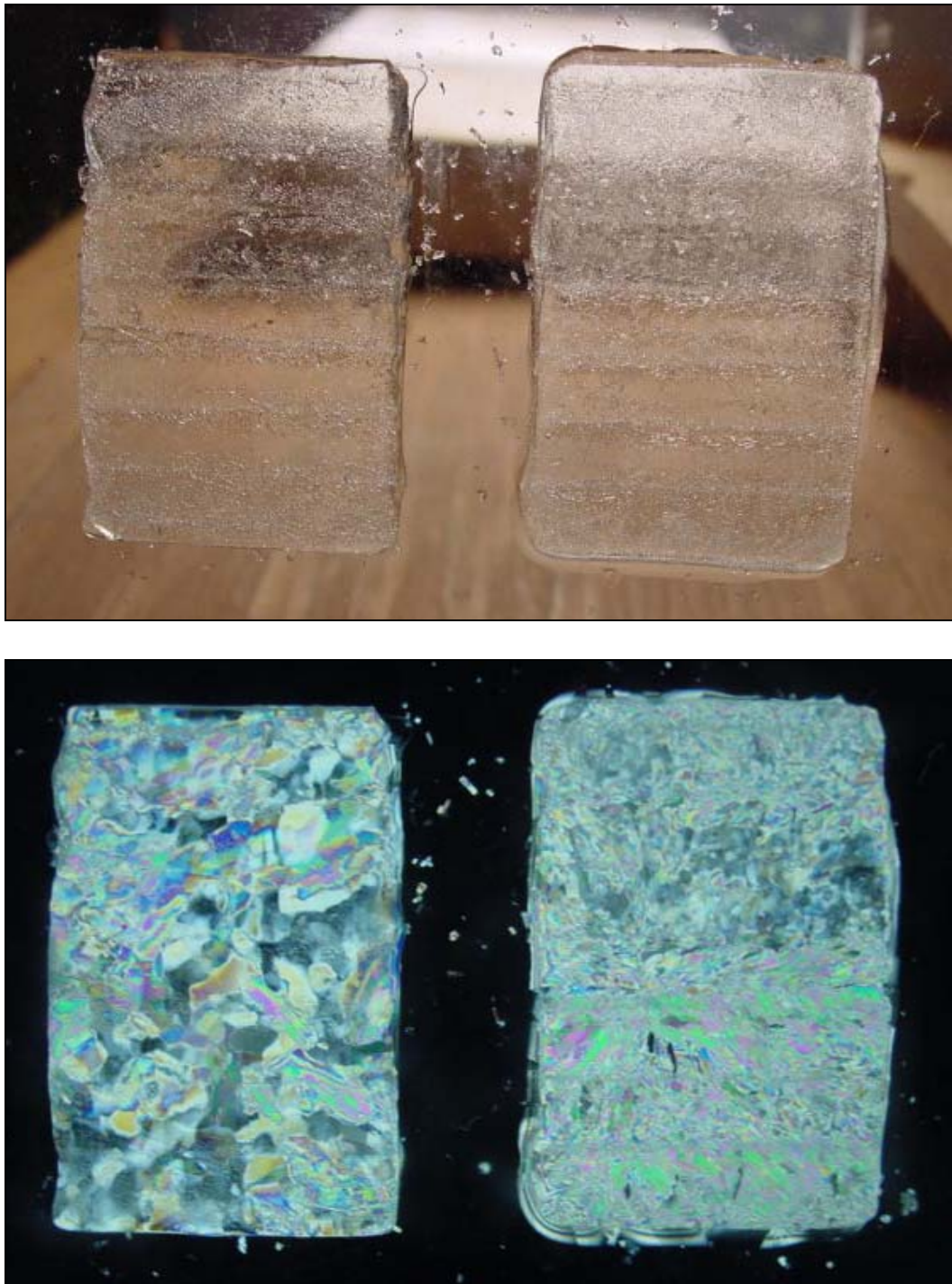


Figure 28. Ice samples from two sides of mold NC with general backlighting (top) and cross-polarized light (bottom). The samples were 1 in. (2.5 cm) wide.



Figure 29. Ice samples from two sides of mold M4-2(5) with point backlighting (top) and cross-polarized light (bottom).

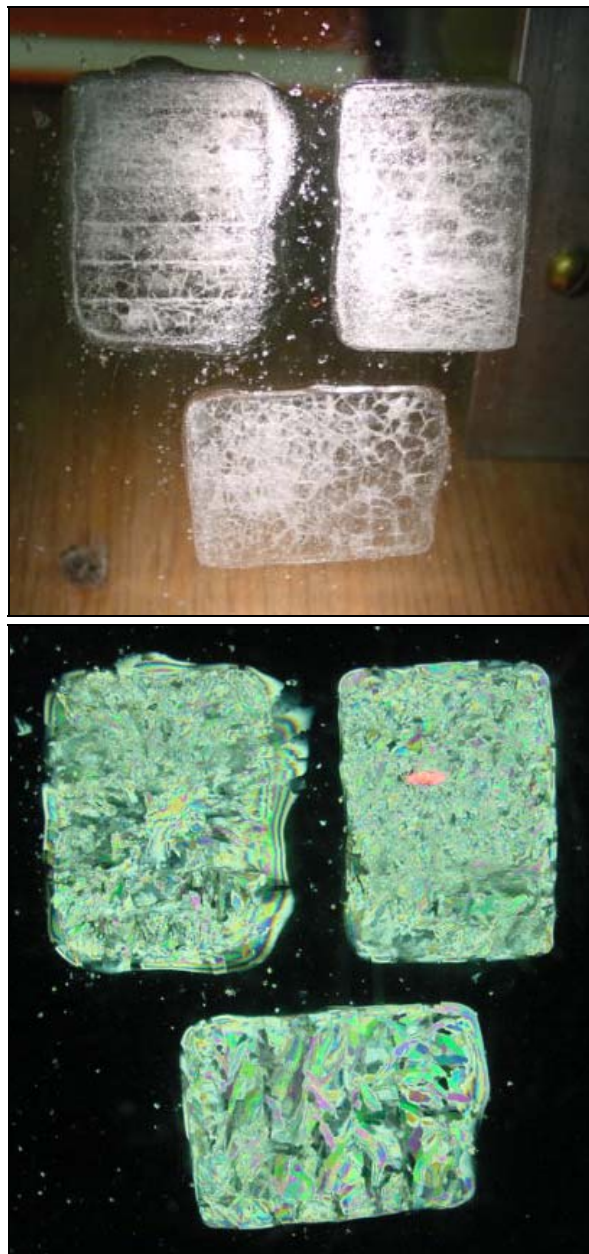


Figure 30. Ice samples from two K molds with point backlighting (top) and cross-polarized light (bottom).

ice from two different molds. The much greater fracture density of these samples, resulting from DLS testing, is very evident in the backlit photograph. As before, the samples display complex, fine-grained ice having a range of sizes.

Thin sections revealed visible differences in ice fracture between these three test conditions, as well as spatial differences in air bubble concentration within and between samples. The cross-polarized views of

the ice revealed complex fine-grained structures with a wide range of grain sizes and significant differences between the two sides of a single test specimen. Each of these structural differences likely contributes to variable adhesion strength among otherwise similar uncoated samples when ice fracture is the dominant failure mechanism.

12 Contact Angle and XPS Analyses

Seven contact angle measurements were performed on each of two coupons of the M4, M42, and MT groups after all test cycles were completed. Photographs of selected droplets on a coupon from each group are presented in Figure 31, where differences in contact angle are clearly visible. The pairs of droplets shown represent a near-maximum and a near-minimum contact angle for that coupon. The data were consistent

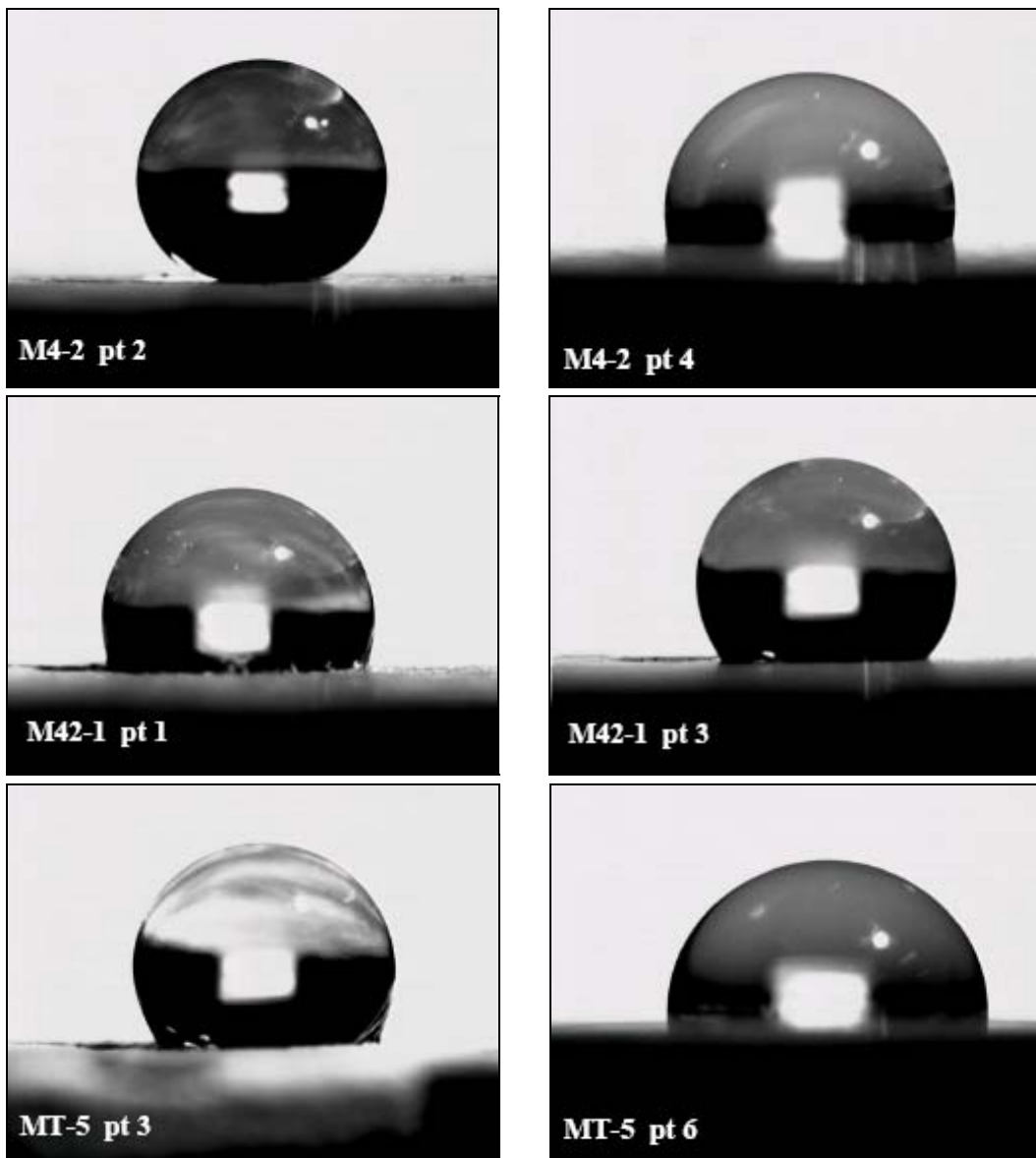


Figure 31. Near-minimum and near-maximum contact angles for coupons M4-02 after five test cycles (top), M42-01 after four test cycles (middle), and MT-05 after four test cycles (bottom).

when the seven measurements for each coupon were grouped as the two highest and the remaining five; the results of these groupings are presented in Table 9. The M4 and M42 high 2-point averages of 135–150° are consistent with data for similar coatings presented by Ferrick et al. (2006), but separate from corresponding MT averages of 103° and 116°. The individual M4 and M42 2-point values were in good agreement, while the differences were greater for corresponding MT data. The 5-point averages indicate significant contact angle degradation from the 2-point averages as a result of testing, 120–123° for SILC and 91–94° for SILC with UVA. The M4 and M42 contact angle averages were very consistent between coupons and with each other, while the MT averages clearly separated from them. Comparing 2-point and 5-point results indicates that surface abrasion from testing reduces the hydrophobic property of the coating. UVA as a component of the SILC also reduces the contact angle and hydrophobic character of the coating and implies important differences in surface conditions, contradicting the similarity inferred from DLS load traces (Fig. 22).

Table 9. Contact angle summary.

Coupon	Low 5-pt average ± std dev (°)	High 2-pt average (°)
M4-02	122 ± 13	150
M4-03	120 ± 9	135
M42-01	123 ± 14	150
M42-02	120 ± 16	149
MT-04	91 ± 5	103
MT-05	94 ± 1	116

X-ray photoelectron spectroscopy (XPS) is a surface analysis method that measures the chemical composition of the outermost 100 Å of a sample. All elements except for hydrogen and helium can be detected at concentrations above 0.05 to 1.0 atom %, depending on the element. In addition, chemical bonding information can be determined from detailed analysis. Trigwell and Calle (2006) reported XPS measurements of fluorocarbon, the principle component of the Rain-X – MP55 coating, remaining on the surface of coupons following three cycles of testing.

XPS measurements were repeated for this study at a pair of points on coupons M4-02, M42-01, and MT-04 after five, four, and four cycles, respectively, in addition to a single point on a Koropon control. One of these measurement points on each coupon was located in the center of the tested area, while the other was located outside this area. Contrary to intuition, the M4 test area data are farther from the control values than the untested area data. The opposite trend generally holds for M42 and MT data. The tested area of the M4 coupon had the highest fluorocarbon measurement of this group, consistent with superior DLS ice adhesion results, while measurements of untested areas of M42 and MT had more fluorocarbon than their tested areas. The XPS measurements, summarized in Table 10, clearly separate the surface condition of the MT coupon from those of the M4 and M42 coupons. MT values always fall between those of the plain SILC coupons and that of the control. The XPS and contact angle surface measurements are consistent with each other, both showing significant differences between MT and M42. While the surfaces clearly differ after multiple test cycles, the ice adhesion characteristics of the M42 and MT coatings are very similar after cycle 1. The small quantity of fluorocarbon on the surface of the MT coupon is inconsistent with comparable or better DLS measures than those of M42. This inconsistency between the DLS and surface measurements highlights the need for additional testing and analysis.

Table 10. XPS data summary (relative atomic concentrations %).

Coupon	F (max, min)	C (max, min)	O (max, min)	N (max, min)	C-H/C-F (max, min)
M4-2	52.4, 40	42.3, 37.4	13.5, 7.7	0.7, 0.0	69/31, 52/48
M42-1	47.5, 33.3	48.2, 39.0	14.2, 10.7	1.4, 0.8	80/20, 60/40
MT-4	14.8, 7.7	66.9, 63.5	19.2, 16.3	3.0, 2.9	98/2, 95/5
Control	0.0	75.3	19.4	4.4	100/0

13 Conclusions

The goals of this experimental program were to optimize the effectiveness of an icephobic coating on the adhesion of ice to different surfaces on the shuttle, to evaluate the effect on ice adhesion of adding a carefully selected UVA to the coating, and to evaluate the consistency of coating performance and its durability. The program included 20 DLS tests, structured in two phases. Each test quantified the adhesion performance of a group of samples at a constant temperature of -112°C (-170°F). These ice samples were grown under carefully controlled conditions at -10°C before being subjected to cryogenic temperatures.

Phase 1 tests focused on determining an optimal coating by measuring the adhesion of ice to several mixes of Rain-X with different weight fractions of the PTFE powders MP-55 and UF-8TA. Ice adhesion to the UF-8TA coating variations was not significantly different from that of the controls. Also, a PTFE mixture of MP-55 and UF-8TA with Rain-X produced an increase in ice adhesion compared to a coating with the same quantity of MP-55 and no UF-8TA. These results show that UF-8TA mixed with Rain-X does not provide an effective icephobic coating. Conversely, phase 1 tests verified that Rain-X mixed with MP-55 was an outstanding coating for reducing ice adhesion to Koropon-coated aluminum at cryogenic temperatures. Decreasing amounts of coating were lost from the coupon surfaces following each successive test cycle, indicating repeated failure in the coating. The ice adhesion performance measures for three cycles of phase 1 testing showed that M4 was the best and most consistent coating by a wide margin, and it was used as the basis of all phase 2 mixes.

The objectives of the phase 2 investigations were to verify the ice adhesion effectiveness and durability of the optimal coating for additional surfaces of potential application on the shuttle, and to quantify any change in effectiveness through multiple test cycles resulting from the addition of the UVA. The results verified the optimal performance and durability of the M4 coating through five cycles of ice growth and adhesive failure. The measurements for the coated coupons with Koropon, Kapton tape, Kapton film, and Fire-X surfaces were a small fraction of the corresponding values for uncoated coupons, demonstrating the generalized effectiveness of the coating. The only loss of ice adhesion performance from adding the UVA

to the SILC, evaluated by comparing the performance of coatings with 8% (MT), 4% (MT4), and 0% (M42) UVA, was reflected in high peak loads in cycle 1. The M42, MT4, and MT load traces were remarkably similar in cycle 2 and higher, implying that the solvent in the UVA may have been largely removed in the first cycle. Additional analysis of these coupons for changes within the coating is needed. Over-mixing and associated Rain-X solvent loss during coating preparation caused a greater increase in ice adhesion to the coating than that of adding the UVA. The “rapid mixing” procedure detailed in this report should minimize this solvent loss and provide consistently optimal coating performance.

Ice fracture occurs from induced thermal stresses during cooling to cryogenic temperatures, and additional fractures are induced during DLS testing of samples without effective coatings. Selected samples were removed from the DLS molds and mounted on glass slides, and thin sections were prepared on a microtome. The thin sections revealed visible ice fracture differences between ice specimens as grown and ice specimens that had been cooled to -112°C and tested, both with and without an effective coating. Spatial and overall differences in air bubble concentration within a sample and between samples were also evident. Cross-polarized views of the ice revealed complex fine-grained structures with a wide range of grain sizes. Each of these structural differences contributes to variable adhesion strength among uncoated DLS samples where ice fracture is the primary failure mechanism.

Contact angle results indicated that both surface abrasion from testing and UVA as a constituent reduce the hydrophobic character of the SILC. Contact angle reduction with the UVA implies differences in surface conditions. XPS measurements of MT always fell between those of the M4–M42 coupons and those of the control, clearly separating the surface condition of the coating with UVA from that without. Consistent XPS and contact angle surface measurements indicate significant differences between the MT and M42 coatings after multiple test cycles. These differences in surface conditions with the addition of the UVA are in contrast to very similar ice adhesion measures after cycle 1. Specifically, the fluorocarbon deficiency on the surface of the MT coating is inconsistent with DLS measures that are close to or better than those of M42. Superior DLS ice adhesion measures for M4 were consistent with maximum XPS surface fluorocarbon measurements after multiple test

cycles. The inconsistency between complementary DLS and surface measurements highlight the need for additional testing and analysis.

The testing and analysis detailed in this report shows that SILC disrupts the ice bond with many substrate materials and may provide early ice liberation during launch for areas on the shuttle system where that characteristic is desired. The hydrophobic nature of SILC may also reduce ice accumulation for areas of the external tank where condensation and rundown contribute to ice growth. The “rapid mix” coating preparation and foam brush application methods detailed here should provide reproducible surface coverage and consistently superior ice adhesion performance. The results of this study also suggest the need for follow-up studies. The reactivity between the UVA and other SILC components is not well understood, and knowledge of the distribution of the UVA within the coating and its relationship to ice adhesion performance should be refined. Expanded DLS testing is needed to confirm the relative adhesion performance obtained for small sample sets in this study and should be combined with analytical methods to characterize the effects of cycling on changes in the residual coating composition.

References

ASTM D3528-96 (2002) Standard test method for strength properties of double lap-shear adhesive joints by tension loading.

Deweese, D., M. Prince, K. McDougal, S. Davis, S. Chandler, and E. Martinez (2006) Developmental tests of the relative performance of coatings on reducing ice adhesion strength. Huntsville, AL: NASA Marshall Space Flight Center.

Ferrick, M.G., N.D. Mulherin, R.B. Haehnel, B.A. Coutermash, G.D. Durell, T.J. Tantillo, T.L. St.Clair, E.S. Weiser, R.J. Cano, T.M. Smith, and E.C. Martinez (2006) Double lap shear testing of coating modified ice adhesion to liquid oxygen feed line bracket, Space Shuttle external tank, ERDC/CRREL TR-06-11. Hanover, NH: U.S. Army Engineer Research and Development Center, Cold Regions Research and Engineering Laboratory.

Trigwell, S., and C.I. Calle (2006) Surface analysis of icephobic coatings. ESPL-TR06-001. NASA Kennedy Space Center.

REPORT DOCUMENTATION PAGE

Form Approved
OMB No. 0704-0188

Public reporting burden for this collection of information is estimated to average 1 hour per response, including the time for reviewing instructions, searching existing data sources, gathering and maintaining the data needed, and completing and reviewing this collection of information. Send comments regarding this burden estimate or any other aspect of this collection of information, including suggestions for reducing this burden to Department of Defense, Washington Headquarters Services, Directorate for Information Operations and Reports (0704-0188), 1215 Jefferson Davis Highway, Suite 1204, Arlington, VA 22202-4302. Respondents should be aware that notwithstanding any other provision of law, no person shall be subject to any penalty for failing to comply with a collection of information if it does not display a currently valid OMB control number. **PLEASE DO NOT RETURN YOUR FORM TO THE ABOVE ADDRESS.**

1. REPORT DATE (DD-MM-YYYY) December 2006		2. REPORT TYPE Technical Report		3. DATES COVERED (From - To)	
4. TITLE AND SUBTITLE Double lap shear testing of coating-modified ice adhesion to Space Shuttle component surfaces				5a. CONTRACT NUMBER	
				5b. GRANT NUMBER	
				5c. PROGRAM ELEMENT NUMBER	
6. AUTHOR(S) Michael G. Ferrick, Nathan D. Mulherin, Barry A. Coutermash, Glenn D. Durell, Leslie A. Curtis, Terry L. St. Clair, Erik S. Weiser, Roberto J. Cano, Trent M. Smith, Charles G. Stevenson, and Eloy C. Martinez				5d. PROJECT NUMBER	
				5e. TASK NUMBER	
				5f. WORK UNIT NUMBER	
7. PERFORMING ORGANIZATION NAME(S) AND ADDRESS(ES) U.S. Army Engineer Research and Development Center Cold Regions Research and Engineering Laboratory 72 Lyme Road Hanover, NH 03755-1290				8. PERFORMING ORGANIZATION REPORT NUMBER ERDC/CRREL TR-06-21	
9. SPONSORING / MONITORING AGENCY NAME(S) AND ADDRESS(ES) National Aeronautics and Space Administration				10. SPONSOR/MONITOR'S ACRONYM(S)	
				11. SPONSOR/MONITOR'S REPORT NUMBER(S)	
12. DISTRIBUTION / AVAILABILITY STATEMENT Approved for public release; distribution is unlimited. Available from NTIS, Springfield, Virginia 22161.					
13. SUPPLEMENTARY NOTES					
14. ABSTRACT The goals of this experimental program were to optimize the effectiveness of an icephobic coating for use on several Space Shuttle surfaces, to evaluate the effects of adding an ultraviolet light absorber (UVA) on coating performance, and to assess the consistency and durability of the basic coating and its modifications. The double lap shear test was used to quantify ice adhesion performance at a constant temperature of -112°C (-170°F). The experiments used ice that was grown as strong and consistently as possible before being subjected to the extreme temperature decrease. Standardized coating application with a foam brush provided consistent and reproducible surface coverage. The program included 20 tests subdivided in two phases. Phase 1 focused on determining an optimal coating of Rain-X and varying weight fractions of PTFE powders MP-55 and UF-8TA. Ice adhesion to the UF-8TA coatings was similar to that of the uncoated controls. Conversely, the MP-55 coatings produced large reductions in ice adhesion. Through three cycles of phase 1 testing the M4 coating, a mixture of 60% Rain-X with 40% MP-55, was the best and most consistent by a wide margin. As a result, M4 was the basis of all phase 2 mixes. Phase 2 tests sought to verify the effectiveness and durability of the optimal coating for several surfaces on the shuttle and to quantify any changes in effectiveness resulting from the addition of UVA to the coating. The ice adhesion to coated coupons with Koropon, Kapton tape, Kapton film, and Fire-X (fire-retardant paint) surfaces was a small fraction of the adhesion to corresponding uncoated coupons. Rain-X solvent loss during prolonged coating preparation caused a greater increase in ice adhesion than that of adding the UVA. A rapid mixing procedure was developed to minimize this problem. The M4 coating showed outstanding performance and durability through five cycles of ice growth and adhesive failure.					
15. SUBJECT TERMS Coatings Double lap shear test		Ice adhesion Space Shuttle			
16. SECURITY CLASSIFICATION OF: a. REPORT U			17. LIMITATION OF ABSTRACT U	18. NUMBER OF PAGES 62	19a. NAME OF RESPONSIBLE PERSON
b. ABSTRACT U					19b. TELEPHONE NUMBER (include area code)
Standard Form 298 (Rev. 8-98) Prescribed by ANSI Std. Z39-18					